Design of an Autothermal Blue Hydrogen Production Plant

A Technical Report submitted to the Department of Chemical Engineering

Presented to the Faculty of the School of Engineering and Applied Science
University of Virginia • Charlottesville, Virginia

In Partial Fulfillment of the Requirements for the Degree
Bachelor of Science, School of Engineering

Brenna Bartholomew

Spring, 2023
Technical Project Team Members
Collin Barbosa
Jack Carroll
Jonathan Paul
Alex Ton

On my honor as a University Student, I have neither given nor received unauthorized aid on this assignment as defined by the Honor Guidelines for Thesis-Related Assignments

Eric Anderson, Department of Chemical Engineering

TABLE OF CONTENTS

1. Executive Summary

Hydrogen production from natural gas is an extremely CO_2 emission-heavy process; however, utilizing carbon capture techniques, this important resource can be produced with a much lower environmental impact. We propose an autothermal methane reforming plant as a relatively low-energy intensive process for the purpose of producing hydrogen and capturing the generated carbon dioxide. Hydrogen will be produced through a series of reactions combining either steam and methane or steam and carbon monoxide to produce hydrogen and carbon dioxide via steam methane reforming reactions or water gas shift reactions, respectively. Carbon dioxide will be captured and sold for use in enhanced oil recovery while hydrogen will be purified via pressure swing adsorption and then sold and piped to an adjacent ammonia production facility.

The plant is expected to run for about 20 years at an average production capacity of 254 kT hydrogen per year. Using Aspen Plus simulations, each unit was designed, and reactions and separations were modeled. From these designs, the overall calculated capital cost of plant installation was estimated at $1.3 billion and operational costs of $567 million. The majority of these operational costs come from raw materials, such as natural gas and oxygen, with labor and utility costs making up a small portion. In total, the yearly revenue of the plant is estimated to be $1.4 billion, made primarily from the sale of hydrogen at $5 per kg and carbon dioxide at $34 per tonne. Based on our analyses of our costs and revenue streams, we have found this to be a feasible and profitable investment that, with proper monetary aid, can begin to move forward with construction. Future blue hydrogen processes could work to further optimize reactor systems towards methane conversion and minimize energy costs associated with carbon capture, and assumptions around unit outputs could also be reevaluated in more detail. Overall, we

believe that our study and design will contribute knowledge to the blue hydrogen space and draw potential investors to its market, leading to a more environmentally friendly hydrogen market.

2. Introduction

One of the greatest challenges mankind faces today is the global climate crisis. According to Lindsey & Dahlman (2022), "by the end of this century, global temperatures will be at least 5 degrees Fahrenheit warmer than the 1901-1960 average, and possibly as much as 10.2 degrees warmer." Temperature increases of this magnitude will have catastrophic consequences on the environment, including rising sea levels and an increase in extreme weather events, such as hurricanes, heat waves, and wildfires. Swift action is needed to reduce greenhouse gas emissions to mitigate global warming, and alternative energy sources to fossil fuels will be critical to the future of our planet. A promising alternative energy candidate is hydrogen due to its accessibility, efficiency in power generation, and minimal emissions. Hydrogen can be produced from common materials, such as methane and water, and can be utilized in a fuel cell to generate electricity without the need for combustion.

Traditional hydrogen production is often called "gray hydrogen" because it produces dirty pollutants and greenhouse gasses that are harmful to the atmosphere. Hydrogen is primarily created through steam-methane reforming (SMR), a process that converts natural gas into hydrogen, and produces carbon dioxide as a byproduct (Yu et al., 2021). The carbon dioxide (CO_2) is released into the atmosphere, contributing to more greenhouse gas emissions. In contrast, "blue" hydrogen captures the CO_2 it produces, decreasing the environmental impact of the process. Blue hydrogen production is the focus of the technical project, and is an excellent step forward in the path towards cleaner energy. In the report below, we outline the design of a blue hydrogen production plant, including the starting materials required, products formed, our

proposed production scale, a process overview, and a brief economic analysis. This process has the ability to produce large amounts of hydrogen while maintaining a relatively low rate of carbon emissions, making it an attractive choice for transitioning to renewable energy.

3. Background and Motivation

Due to the variety of operations utilized in this production facility, this process had to be adapted from a wide range of literature studies, organized, and integrated into one seamless process. While autothermal reforming (ATR) is not a new technology, its implementation is still limited, so there are few sources describing the conditions of a full-scale facility including ATR, water-gas shift (WGS) reactors, multiple amine scrubbers, and pressure swing adsorption (PSA). Information for each of these processes was instead drawn from literature describing the individual units, and economical data was drawn from different processes with identical output products.

A combination of ATR and WGS reactors for hydrogen production was chosen based on a comparative study of the different forms of blue hydrogen production conducted by Oni et al. (2022). This paper provides a holistic study of blue hydrogen production, from the impacts of plant size and technologies on hydrogen production and carbon capture, to economic preferability of different production technologies. Those considered in this paper are SMR, ATR and natural gas deposition (NGD). The findings of this paper showed that a production capacity of about 600 tonnes of hydrogen per day was most economically favorable, and of the production techniques considered, at the current market values of natural gas and hydrogen ATR outperforms all others. Furthermore, when considering greenhouse gas emissions, ATR also has the lowest lifetime emissions at around 3.9 kg CO_2 eq/kg H_2. Our design builds off the design used in Oni et al. (2022), further specifying exact natural gas compositions to be used and

providing a more thorough and exclusive economic analysis directed at our specific production facility and location that includes sale of CO_2 and H_2S as a supplement to H_2 sale.

The ATR design was based on a paper by Xu and Froment (1989) that developed a kinetic model of each reaction that occurs within the reactor. This paper outlines the temperature dependent rate equations that properly describe the reactions occurring in parallel over the $Ni/MgAl_2O_4$ catalyst developed by this research team. These reactions include oxidation, steam methane reforming, and a water gas shift reaction. The paper further provides an estimate of the best model parameters, including operating temperature and pressure, obtained through thorough analyses of computational and experimental data. In order to simulate these reactions for our feedstock and conditions, we adapted the kinetic models and catalytic parameters to the Aspen Plus process simulator, assuming conversions of larger hydrocarbons, such as ethane, butane, and propane, were of the same kinetics as methane. Furthermore, reactor dimensions were determined by optimizing hydrogen production and minimizing methane output. We also used the defined "best model" as a starting point for optimizing our reactor efficiency and opted to use the same $Ni/MgAl_2O_4$ catalyst that was developed by Xu and Froment.

Two papers were consulted in the kinetic design of the WGS reactors. The catalyst and reaction rates for the high temperature (HT) reactor were derived from a model developed by Hla et al. (2009) while those of the low temperature (LT) reactor were adapted from Ayustuy et al. (2004). Hla et al. models the WGS reaction over an iron-chromium based catalyst at 450 $^\circ$C and accounts for feed compositions typically found in bed gasification reactors and methane reforming units. The paper found that iron-chromium based catalysts provide a very high CO shift when compared with other catalysts, and also determined that there was no inhibitory effect from high CO_2 concentrations, such as those in the ATR outlet stream. Due to the high degree of

similarity of feed compositions used in this paper to our ATR outlet product stream compositions, we opted to utilize the rate equations and catalyst developed by this study to simulate the reactions occuring in the HT WGS reactor. The paper used to model the LT WGS reactor, written by Ayustuy et al. (2004), developed a temperature dependent rate equation for a plug-flow WGS reactor operating between 180ºC and 217ºC packed with a $CuO/ZnO/Al_2O_3$ catalyst. In comparing this catalyst to other known catalysts used in WGS reactors, Ayustuy et al. (2004) found that the required activation energy was between 25 and 125 kJ/mol lower, thus increasing the rate of reaction in a cooler unit. As with the HT WGS reactor, we adapted the kinetic model developed in this reactor along with the conditional parameters to Aspen Plus to simulate the conversions taking place in this part of our system of reactors.

The PSA unit design was adapted from a patent by Baksch et al. (2002), developed expressly to separate materials such as CH_4, N_2, CO_2, and CO from an H_2 stream. The PSA outlined by the patent consists of a four-bed system with sequential pressurization, depressurization, purge, and repressurization between the beds, allowing for repressurizations to be mechanically aided by the depressurization of another unit. Each bed is layered with three different catalysts from bottom to top: alumina, activated carbon, and zeolite. The complete PSA cycle described in this patent consists of 16 steps, with a valve system included to optimize the connections between the four beds. This design also claims to provide higher hydrogen recovery alongside a lower adsorbent inventory. The basis for component separation within the PSA unit was modeled after a study by Yavari et al. (2016) that describes the reactor number and size required for complete H_2 separation. Based on these studies and the product streams of our process, we opted to use two 4-bed reactors operating independently of each other, packed with the same layered catalysts as depicted in the patent by Baksch et al. With this design, our process

variables are held very similar to those of the separation study, and the reactor design is identical to that of the patent, ensuring that our assumed separation will be the same as that modeled in each of these studies.

Two amine scrubbers are utilized in our process: AS1, which removes the H_2S from the natural gas feedstock, and AS2, which removes most of the carbon dioxide from our product stream. A study by Jassim (2016) was used to develop the most optimized process by which to remove H_2S in AS1. This paper utilizes the Aspen HYSYS amine package to computationally determine the most optimized conditions for H_2S removal from a stream containing CO_2 at temperatures ranging from 45 to 65ºC and pressure ranging from 50 to 220 kPa. MDEA concentration was also optimized with values ranging from 15 to 50 wt% MDEA. Our process adapted the simulation developed in this paper for use in Aspen Plus, rather than Aspen HYSYS and used the optimal conditions as outlined in Jassim's study to maximize H_2S removal and minimize operational energy costs. The second amine scrubber design was adapted from a previous University of Virginia chemical engineering capstone project that required the capture of CO_2 from power plant emissions (Lange et al. 2020). The process outlined by this group set out the Aspen Plus design, which we then adapted to our process conditions, altering only the input feed stream composition and flow rate in order to correctly simulate our process outputs.

To supplement our plant design, we also performed an in-depth economic analysis of our proposed process in order to determine its real-world feasibility. This analysis used cost estimates from a wide variety of online sources to determine costs per unit of natural gas, oxygen, catalysts, amines, process water, electricity, and steam, most of which were adapted from Turton et al. (2012). These values were combined with flow rate estimates conducted in Aspen Plus to obtain yearly operational cost estimates. Similarly, capital costs of the plant were

estimated using the CAPCOST Excel spreadsheet, provided by Turton et al. (2012), which takes process unit parameter inputs designed in Aspen Plus modeling software to provide an estimate of the initial capital cost of the project. Labor costs were also considered; again, Turton et al. was used to estimate the required number of operators who were then assumed to be paid the average hourly rate of a chemical plant operator. Furthermore, to increase the credibility of our plant design we calculated simple payout periods, IRR, and cumulative DCF values for a wide range of possible circumstances, including doubled and tripled natural gas prices and decreased hydrogen prices. Taxes, deductions, depreciation, and loan financing were all included in this analysis with values taken directly from the Federal Reserve (2023) or estimated based on the assumption of a plant location in Midland, Texas.

4. Final Design

4.1 Process Overview

Our process is made up of six main stages: sulfide removal via amine scrubbing, autothermal reforming, water-gas shift reaction, CO_2 removal via amine scrubbing, CO_2 compression, and H_2 purification via pressure swing adsorption. The feed to this process is natural gas from Midlands, TX and the main product is H_2 with a purity of 99.99%, as well as CO_2. Figure 4.1-1 provides a block flow diagram for this process.
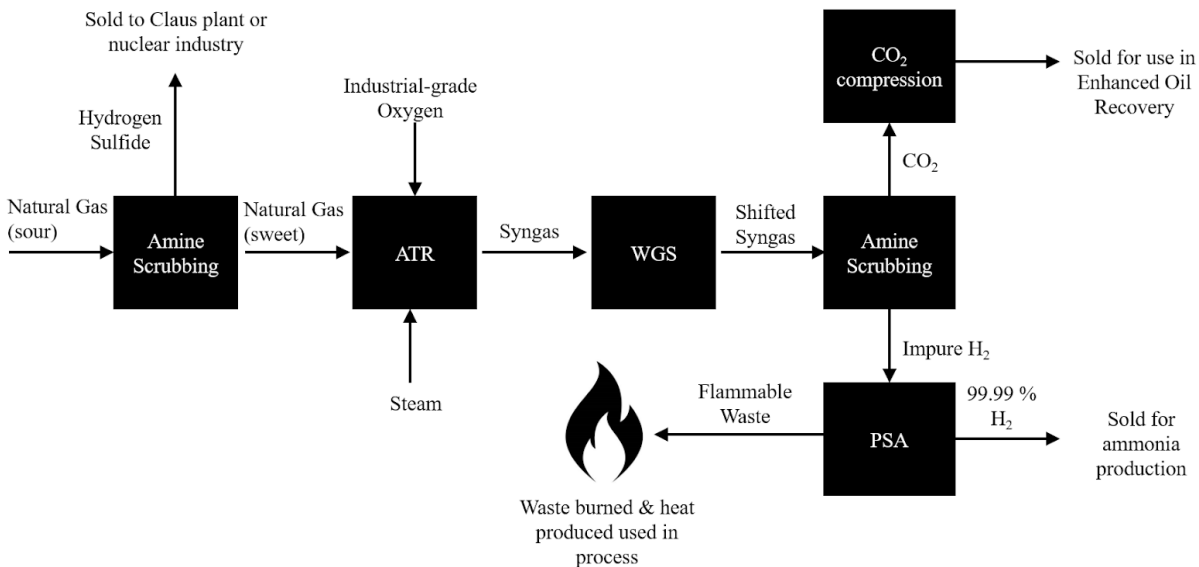
Figure 4.1-1 Block flow diagram of overall blue hydrogen production process

4.2 Feedstock Characterization

The feedstock for this process is natural gas supplied by the Permian Highway Pipeline in Midlands, TX. The gas is assumed to be "sour," which is defined by the state of Texas as containing at least 24 ppm of hydrogen sulfide (H_2S) (*Sour Gas Handling Compliance*, n.d.). Sour gas was chosen to reduce raw material costs, as it is typically cheaper than sweetened natural gas. For this project, the gas stream was assumed to contain approximately 52 ppm H_2S, or about 0.005 mol%, in order to be non-negligible. An exact composition of natural gas from Midland, TX could not be determined, so a molar composition was estimated based on typical sour natural gas and gas taken from the Permian Basin area Additionally, a feed stream of 59,218 kg/hr was established to meet our production goal of 600,000 kg H_2 per day. Table 4.2-1 summarizes the mole percentages, mass percentages, and mass flows of the feed stream.

Table 4.2-1 Assumed composition of natural gas feedstock

Component	Mole %	Mass %	Mass Flows (kg/hr)
CH_4	75	57.82	86,072
C_2H_6	10	14.45	21,512
N_2	7	9.42	14,029
C_3H_8	4	8.48	12,619
C_4H_{10}	2	5.59	8,316
CO_2	2	4.23	6297
H_2S	0.005	0.008	12
Total	100	100	148,856

4.3 Amine Scrubbing for Hydrogen Sulfide Removal

The amine scrubbing unit consists of two primary columns: an absorber and a stripper. The absorber serves to intake the feed sour gas and output sweetened gas. The stripper column serves to recycle the amines by removing the sweetened gas and eventually recycling the amines to save costs. The feed sour gas enters the adsorber at the bottom while the clean lean amines enter at the top of the column. No reboiler or condenser is required for this column. H_2S and CO_2 are removed from the gas phase and absorbed into the amines converting them to rich amines. The now sweet gas exits the top of the absorber and continues through the process to the autothermal reformer. The rich amines enter the stripper at the top of the column at stage 3. In the stripper, almost opposite reactions occur compared to the absorber. Now a rich amine feed is fed into the column and H_2S and CO_2 ions move into the gas phase and exit the column. The gas phase enters a partial-vapor condenser and the sour gas exits the system to be sold to a Klaus plant for sulfur production. At the bottom, the now lean amine solvent enters a total kettle

10

reboiler and moves to be fed back to the top of the absorber. Some amine solvent is expected to be lost in the system so outside solvent will have to be continually added. There is still a generous heat requirement for the system, however there is an opportunity for heat recycling. Lean amine coming out of the stripper reboiler must be cooled and condensed to be fed to the top of the absorber. Rich amine coming from the bottom of the absorber must be heated anyway in the stripper. A cross-heat exchanger between these two streams may be used to reduce external heating requirements. A PFD for this unit is given in Figure 4.3-1.
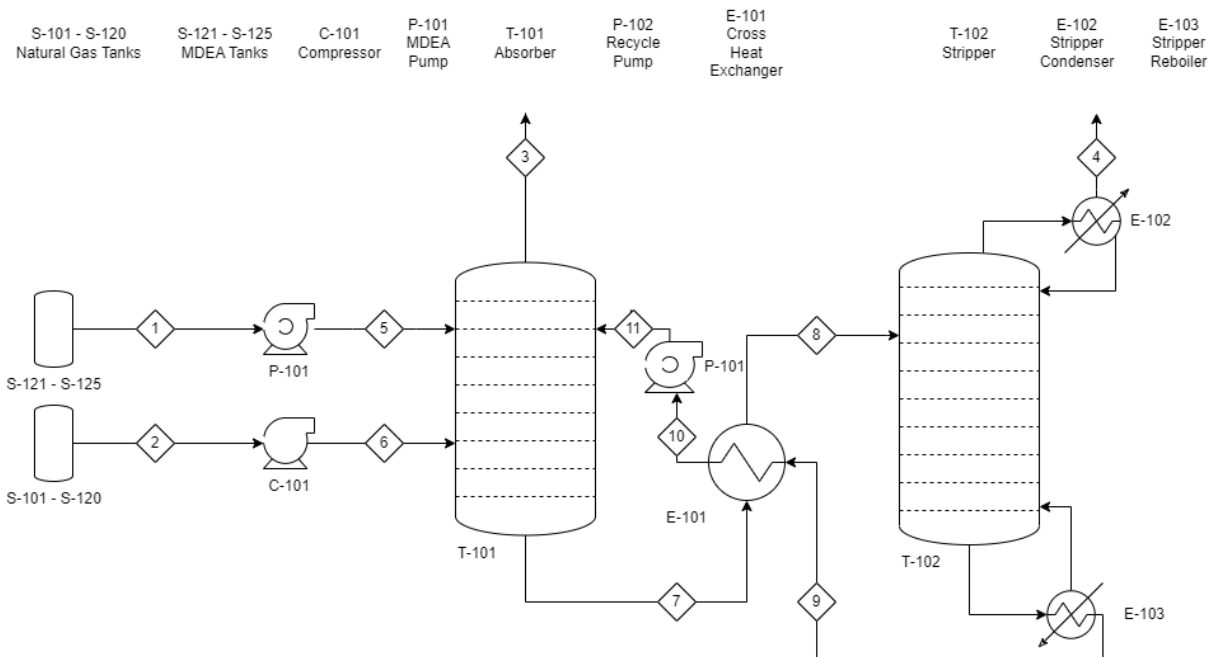
Figure 4.3-1 PFD of first amine scrubbing unit for hydrogen sulfide removal

Natural gas feed enters the absorber at 50°C and 4742 kPa. Amine feed enters the absorber at 50°C 4620 kPa. Sweet natural gas exits the top 63°C and 4620 kPa. Saturated amines exit the bottom at 58°C and 4680 kPa. The absorber itself has 10 stages and no reboiler or condenser. The sieve trays are spaced 0.61 meters apart making the column 6.1 meters high with a diameter of 2.0 meters. The column operates between 63°C and 73°C and at pressures between 4620 kPa to 4680 kPa.

The bottoms from the absorber enters the stripper at 58°C and 4680 kPa. Sour gas exits the top of the striper at 40°C and 200 kPa. The bottoms of the stripper exits at 125°C and 220 kPa. The stripper operates with 18 trayed stages as well as a condenser and reboiler. The partial-vapor condenser operates at 200 kPa and has a -1.76 MW heat duty. There is a kettle reboiler operating with a 12.3 MW heat duty, bottoms rate of 4950 kmol/hr, and a reflux ratio of 1. The trays are 0.55 meters apart with a diameter of 1.4 meters. Stripper internals have a total size of 9.9 meters. The column operates between 40°C and 125°C and pressures between 200 kPa and 220 kPa. Stream results for this unit are given in Table 4.3-1.

Table 4.3-1 First amine scrubbing unit inlet and outlet stream compositions (kg/h)

Component	1	2	3	4	9
H_2O	906	0	813	90	85,159
H_2S	0	11	0	8	0
CO_2	0	5,900	386	5,506	0
MDEA	41	0	1	0	26,422
$MDEA^+$	0	0	0	0	77
HS^-	0	0	0	0	4
HCO_3^-	0	0	0	0	10
CO_3^{--}	0	0	0	0	1
OH^-	0	0	0	0	5
CH_4	0	80,646	80,613	33	0
C_2H_6	0	20,156	20,148	7	0
N-C4	0	7,792	7,791	1	0
N_2	0	13,144	13,141	3	0
C_3H_8	0	11,823	11,820	3	0
Total	947	139,472	134,713	5,650	111,678

4.4 Autothermal Reformer

As shown in Figure 4.4-1, the reactor system of this process consists of an autothermal reformer (ATR) followed by two water-gas shift (WGS) reactors in series. The bulk of the H_2 product is produced in the ATR, while the WGS reactors are used to further produce H_2 from the remaining H_2O and CO and to convert CO into CO_2.
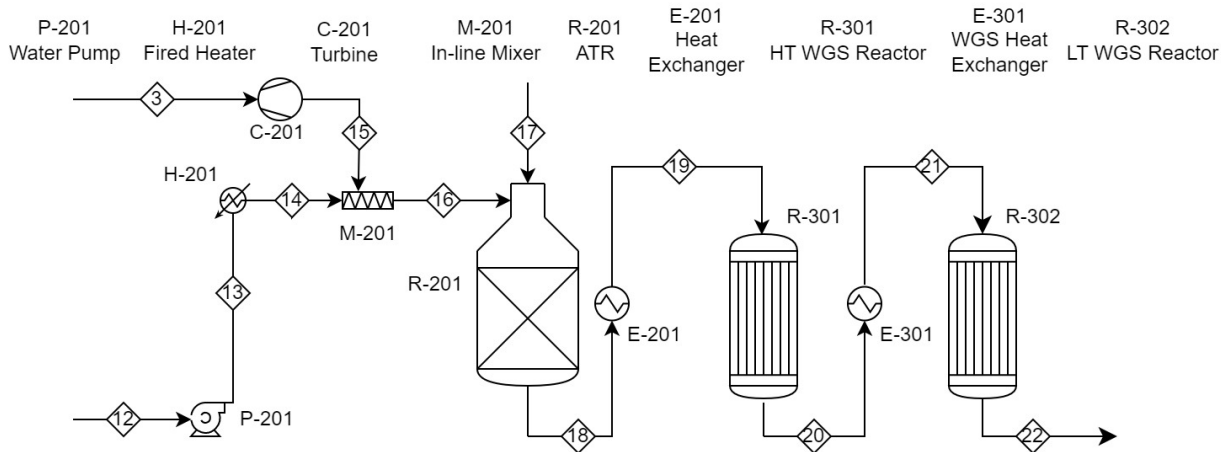
Figure 4.4-1 PFD of autothermal reformer and water-gas shift reactors system

The ATR requires an input stream of methane (in the form of natural gas), steam, and oxygen. These compounds undergo multiple reactions over the ATR's catalytic bed, creating products of CO, CO_2, and H_2. The highly insulated reactor operates at a pressure of 30 bar and temperature of 900 °C and is designed as 25 m tall with a diameter of 4 m. The catalyst used is $Ni/MgAl_2O_4$, which is active in each reaction that takes place within the ATR and is therefore present in the entire length of the unit. A gas product stream leaves the reactor at 29.5 bar and around 680 °C flowing into a heat exchanger to cool it to the operating temperature of the first WGS reactor. The total heat duty of the reactor is 0 MW, held autothermal by the combination of an exothermic combustion reaction and an endothermic methane reforming reaction. Inlet and outlet stream compositions are provided in Table 4.4-1, and the oxygen injection (stream 17) is composed of pure oxygen at a flow rate of 119,676 kg/hr. Stream 16, as depicted in Table 4.4-1

consists of a mixture of the sweetened natural gas from AS1 and stream 14, which is pure steam with a flow rate of 232,397 kg/hr. The small difference in mass input to output of the ATR is due to added H_2 and CO, which are used to satisfy the kinetic equations used in simulation and has a negligible effect on the rest of the process.

Table 4.4-1 ATR inlet and outlet stream compositions (kg/h)

Component	16	17	18
H_2	0	0	30,209
CH_4	80,613	0	12,179
H_2O	233,210	119,676	184,761
N_2	13,141	0	13,141
CO	0	0	104,638
C_2H_6	20,148	0	0
O_2	0	0	0
H_2S	0	0	0
CO_2	386	0	142,189
C_3H_8	11,820	0	0
C_4H_{10}	7,791	0	0
Total	367,109	119,676	487,117

4.5 Water-Gas Shift Reactors

Following the ATR, syngas is sent to a water-gas shift reactor system consisting of a high-temperature (HT) reactor and a low-temperature (LT) reactor separated by a heat exchanger, as shown in Figure 4.4-1. Each reactor is designed similar to a shell and tube heat exchanger to meet heat transfer requirements. Each reactor consists of 750 stainless steel tubes, 10 cm in diameter, and 1.5 m in length. The HT reactor contains an iron-chromium-copper catalyst and

operates at a temperature of 400°C and pressure of 30 bar. A pressure drop of 3.8 bar occurs

through the reactor, with the process stream leaving at about 26 bar. The gas then flows through a

heat exchanger, cooling the stream to 175°C before entering the LT reactor operating at the same

temperature and a pressure of 26 bar. The gas leaves the LT reactor at about 23 bar. The

composition of inlet and outlet streams from each reactor are given in Table 4.5-1.

Table 4.5-1 Water-gas shift reactors stream compositions (kg/hr)

Component	19	21	22
H_2	30,209	37,173	37,740
CH_4	12,179	12,179	12,179
H_2O	184,761	122,522	117,459
N_2	13,141	13,141	13,141
CO	104,638	7,869	0
C_2H_6	0	0	0
O_2	0	0	0
H_2S	0	0	0
CO_2	142,189	294,232	306,603
C_3H_8	0	0	0
C_4H_{10}	0	0	0
Total	487,117	487,117	487,117

Since the water-gas shift reaction is exothermic, heat is generated during this reaction.

The HT reactor generates 36.9 MW of heat and the LT reactor generates 2.54 MW of heat. Heat

is removed using water running through the outer shell of the reactor. Water enters the HT

reactor at 80°C and 60,000 kg/hr and leaves as steam at the same temperature and flow rate. For

the LT reactor, water enters at 155°C and 25,000 kg/hr and leaves as steam at the same

temperature and flow rate. At these conditions, the HT reactor achieved 92.5% conversion of CO

and the LT reactor achieved 100% CO conversion, for an overall system conversion of 100%. For H_2O, the HT achieved 33.7% conversion and the LT achieved 0.04% conversion, for an overall system conversion of 36.4%.

4.6 Amine Scrubbing for Carbon Dioxide Separation

Following the water-gas shift reactors, the now shifted syngas is sent to a second amine scrubbing unit where CO_2 will be separated out. This second amine scrubbing unit consists of an absorbing column, stripping column with reboiler and condenser, one pump, two flash tanks, and two heat exchangers which can be seen in Figure 4.6-1. Impure H_2 flows out of the absorber (stream 5) to the PSA unit, while purified CO_2 with excess water exits the stripper in the distillate (stream 9). That excess water is separated out via V-102, with the final purified CO_2 product (steam 14) going to the compression unit. A CO_2 recovery of 97.5% is achieved, with a purity of 99.5%. As for the impure H_2 product stream, a H_2 recovery of 99.6% is achieved with low purity, but this will be remedied in the PSA unit following this operation.
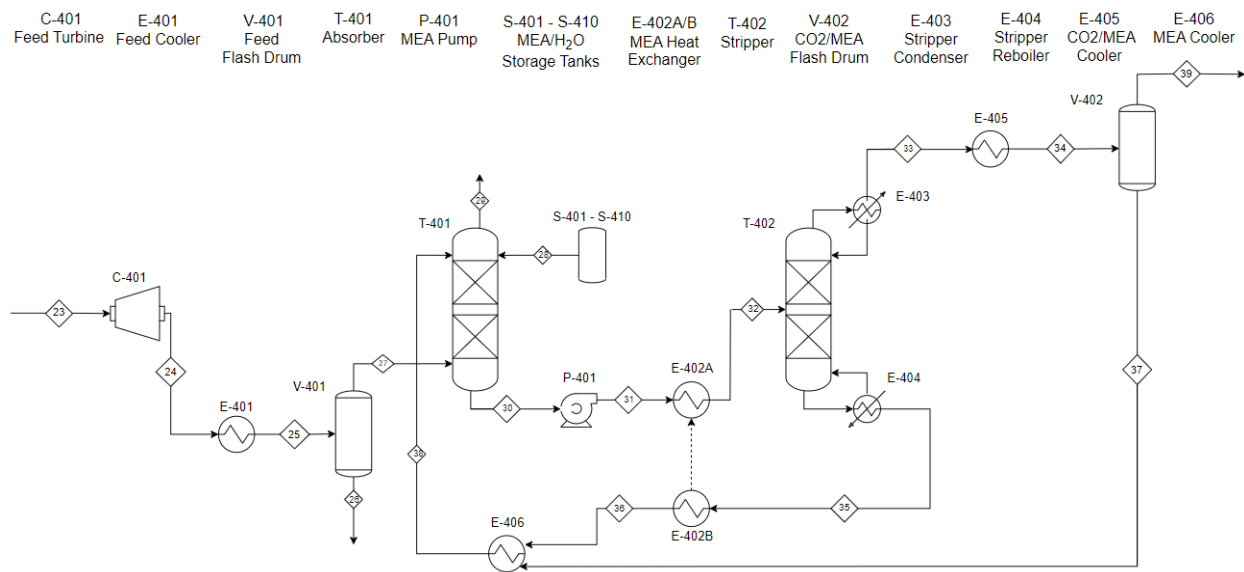
Figure 4.6-1 PFD of amine scrubber for carbon dioxide separation

The absorber contains 4 theoretical packed stages consisting of ⅝" generic metal pall rings, each at an equivalent packing height (HETP) of 3.33 meters. It operates at 8.00 bar of pressure with a pressure drop of 0.0631 bar occurring throughout the column. Diameter for the absorber was determined to be 9.82 meters, under the 10 meter limit set by Professor Anderson. The impure H_2 product stream exits the absorber at a temperature of 74.4°C and a pressure of 8 bar. Composition of inlet and outlet streams for absorption can be seen in Table 4.6-1.

Table 4.6-1 Absorption stream results (kg/hr)

Component	23	24	25	26	27	28	29	30	31	32
H_2	37,740	37,740	37,740	1	37,739	0	37,573	166	166	166
CH_4	12,179	12,179	12,179	0	12,179	0	12,121	57	57	57
H_2O	117,459	117,459	117,458	112,713	4,745	11,640	15,052	2,695,080	2,695,090	2,698,880
N_2	13,141	13,141	13,141	0	13,141	0	13,104	37	37	37
CO	0	0	0	0	0	0	0	0	0	0
CO_2	306,603	306,603	306,602	235	306,367	0	7,514	31,437	31,496	54,398
MEA	0	0	0	0	0	14	14	239,552	239,695	293,287
H_3O^+	0	0	0	0	0	0	0	0	0	0
CO_3^{-2}	0	0	0	0	0	0	0	5,413	5,402	2,585
HCO_3^-	0	0	1	1	0	0	0	68,993	68,973	59,001
MEA^+	0	0	0	0	0	0	0	511,312	511,218	475,991
$MEACOO^-$	0	0	0	0	0	0	0	720,660	720,575	688,306
Total	487,122	487,122	487,122	112,951	374,171	11,654	85,378	4,272,710	4,272,710	4,272,710

In regards to the stripping column, it contains 7 theoretical packed stages consisting of 3.5" generic metal pall rings, each at an HETP of 2.83 meters. This column operates at a pressure of 10 bar with a pressure drop of 0.0885 bar occurring throughout the column. Diameter for the stripper was determined to be 10.7 meters, slightly above Professor Anderson's recommendations but not significantly affecting costs. A kettle reboiler and partial-vapor condenser are also utilized in this column, therefore bringing the total number of stages to 9, with heat duties of 1030 and -205 MW respectively. Reflux ratio was specified at 0.5, along with a

bottoms rate of 3.4 million kg/hr. The purified CO_2 stream exits the process at a temperature of 45°C and a pressure of 10 bar. Composition of inlet and outlet streams for the stripper can be seen in Table 4.6-2. Stream results for the overall separation process are present in Table 4.6-3.

Table 4.6-2 Stripping stream results (kg/hr)

Component	32	33	34	35	36	37	38	39
H_2	166	166	166	0	0	0	0	166
CH_4	57	57	57	0	0	0	0	57
H_2O	2,698,880	567,987	567,882	2,148,650	2,148,730	566,549	2,715,180	1,333
N_2	37	37	37	0	0	0	0	37
CO	0	0	0	0	0	0	0	0
CO_2	54,398	304,106	303,850	65	10	4,996	0	298,854
MEA	293,287	356	0	928,693	928,231	0	913,323	0
H_3O^+	0	0	0	0	0	0	0	0
CO_3^{-2}	2,585	0	0	23	57	0	1,376	0
HCO_3^-	59,001	0	356	1,477	1,167	356	513	0
MEA^+	475,991	0	361	120,950	121,062	361	129,852	0
$MEACOO^-$	688,306	0	0	200,147	200,746	0	212,020	0
Total	4,272,710	872,710	872,710	3,400,000	3,400,000	572,262	3,972,260	300,447

Table 4.6-3 Overall separation process stream results (kg/hr)

Component	23	26	28	29	39
H_2	37,740	1	0	37,573	166
CH_4	12,179	0	0	12,121	57
H_2O	117,459	112,713	11,640	15,052	1,333
N_2	13,141	0	0	13,104	37
CO	0	0	0	0	0
CO_2	306,603	235	0	7,514	298,854
MEA	0	0	14	14	0
H_3O^+	0	0	0	0	0
CO_3^{-2}	0	0	0	0	0
HCO_3^-	0	1	0	0	0
MEA^+	0	0	0	0	0
$MEACOO^-$	0	0	0	0	0
Total	487,122	112,951	11,654	85,378	300,447

4.7 Pressure Swing Adsorption

An 8-bed pressure swing adsorber will further purify the product stream coming from the second amine scrubber to an H_2 purity of 99.99%, working in two blocks of four bed systems. The unit is designed to connect each bed to every other bed, with gate and control valves metering flow between beds. Figure 4.7-1 is a process flow diagram for the full unit, including generalized valve locations and piping layout. The letter at the end of each bed label indicates which four-bed system the bed is part of (A or B).
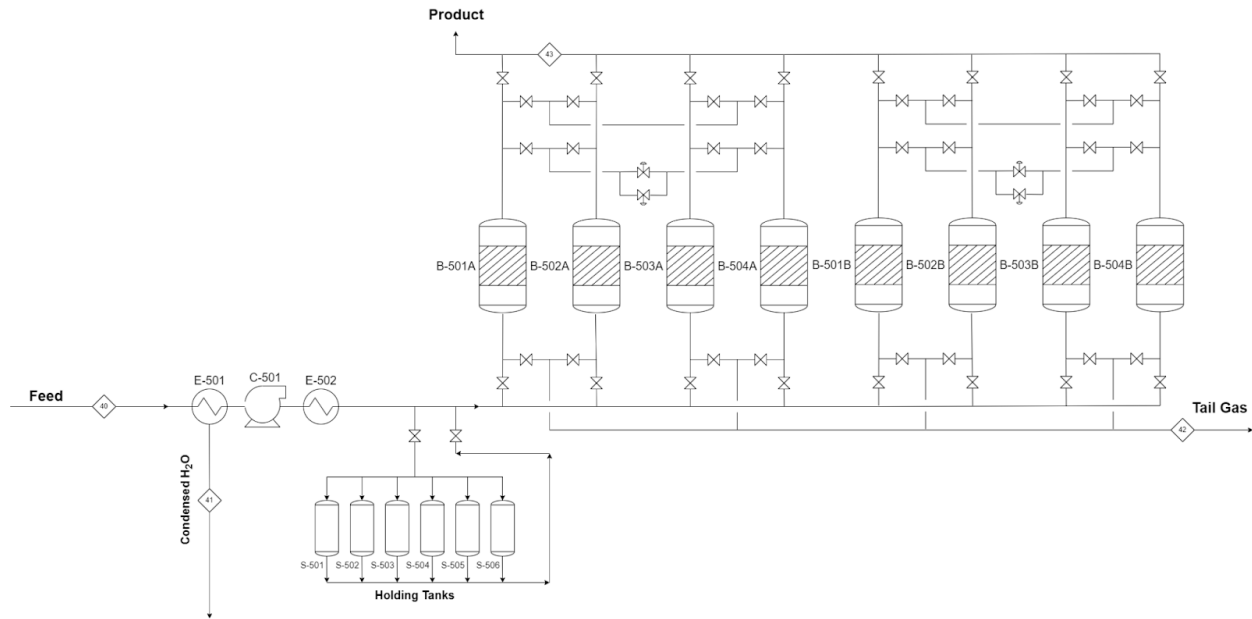
Figure 4.7-1 PFD of PSA unit

Each bed is 6 m in diameter and 18 m in height, and contains about 41% by volume CaX Zeolite, 53% activated carbon, and 6% alumina. The unit operates at an average temperature of 40°C, and does not require additional heat to maintain this temperature. Maximum adsorption pressure is 11.71 bar, and desorption pressure is 1.33 bar. The unit operates at a feed flow of about 76,600 kg/hr, with H_2 recovery at 81.6%. The composition of feed, product, tail gas, and condensed water streams are given in Table 4.7-1. Note that a 100% pure product stream was assumed for simplicity- N_2 will likely be the primary impurity in that 0.01% range due to its molecular size similarity to H_2 compared to other components. Additionally, ~87% of H_2O will be condensed out of the feed stream before entering the unit by a decanter in HE-501, described in Table 4.9-1.

Table 4.7-1 PSA stream results (kg/hr)

Component	40	41	42	43
H_2	37,573	0	6,913	30,659
CH_4	12,121	0	12,121	0
CO	0	0	0	0
CO_2	7,514	0	7,514	0
N_2	13,104	0	13,104	0
H_2O	15,052	13,087	1,965	0
MEA	14	0	14	0
Total	85,378	13,087	45,913	30,659

4.8 Carbon Dioxide Compression

As seen in Figure 4.8-1, compressing the CO_2 gas from the amine scrubber into a liquid will be done with a four-stage centrifugal compressor. This compressor operates at a differential
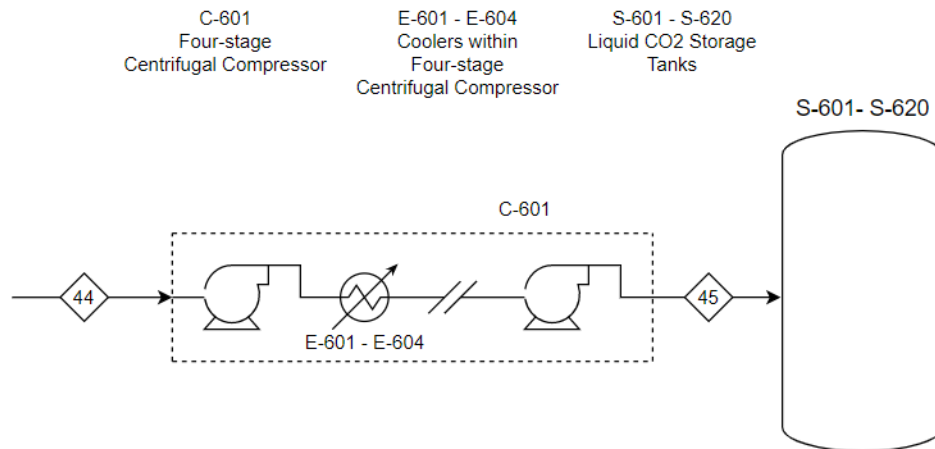
Figure 4.8-1 PFD of carbon dioxide compression unit

pressure of 62.3 bar at a power of 12.4 MW. With these specifications, the gas enters the unit at 48.1°C with 10 bar of pressure, and exits as a liquid at 25°C with a pressure of 72.3 bar. The

3.1°C difference in the product stream of AS2 (stream 39) and the feed stream of this unit (stream 43) is due to different Aspen Plus property methods being used to run the respective simulations. In both cases, the vapor fraction of the streams is 1.

4.9 Ancillary Equipment

Heat Exchangers

12 heat exchangers are used throughout this process. Table 4.9-1 provides a summary of the operating conditions for each heat exchanger, including the process and cooling stream temperatures, pressure, heat duty, and heat transfer area required. Each heat exchanger consists of a shell and tube design, with the process stream flowing through the tube side and water flowing through the shell side. Type 316 stainless steel is used as the material of construction.

Table 4.9-1 Summary of heat exchanger design

Unit	Hot Inlet Temp (°C)	Hot Outlet Temp (°C)	Cold Inlet Temp (°C)	Cold Outlet Temp (°C)	Pressure (bar)	Heat Duty (MW)	Heat Transfer Area (m²)
E-101	124.8	50	15	30	2	-8.85	173
E-102	100.6	39.9	15	30	2	-1.76	47
E-103	270	240	124.4	122.5	2.5	12.27	111
E-201	660	400	15	307.8	5	86.9	278
E-301	400	175	15	152.8	5	73.5	431
E-401	110	40	15	25	8	-91.4	2190
E-402	186	155	79.9	105.4	10	116	2920
E-403	177.5	171.4	15	100	10	-205	2150
E-404	270	240	183.5	186.9	10	1030	17600
E-405	171	45	15	25	10	-422	6770
E-406	139.2	40	15	20	8	-394	22900
E-501	63	30	15	55	8	10.8	200
E-502	64.6	40	15	49.6	11.7	4.07	200
E-601	97.8	33.1	15	25	16.40	-5.91	528
E-602	73.4	33.0	15	25	26.89	-4.21	481
E-603	73.7	33.3	15	25	44.09	-5.01	566
E-604	73.8	25	15	25	72.3	-17.2	827

Pumps and Compressors

Six pumps/compressors are used throughout this process. Table 4.9-2 provides a summary of the operating conditions for each compressor, including type, differential pressure, and power.

Table 4.9-2 Summary of pump and compressor design

Unit	Type	Differential Pressure (bar)	Power (MW)
C-101	Centrifugal	34.47	8.91
P-101	Centrifugal	45.19	0.00145
P-102	Centrifugal	44	0.165
C-201	Centrifugal	-16.2	-1.61
P-201	Centrifugal	24.5	0.191
C-401	Centrifugal	-15.5	-23.9
P-401	Centrifugal	2.00	0.298
C-501	Centrifugal	6.71	5.73
C-601	Centrifugal	62.3	12.4

Fired Heater

A high-pressure, high-temperature pure steam input is required prior to the ATR. A fired heater (H-201) heats pressurized water (stream 13) from 15.1 ºC to 380 ºC at a constant pressure of 30 bar, completely vaporizing the liquid water stream. The net heat duty of this unit is 208 MW, which is provided by burning the waste methane and hydrogen from PSA.

Tanks

6 holding tanks (S-501, 502, 503, 504, 505, 506) are used in the PSA unit, located just upstream of compressor C-501. Each is a cylindrical tank made from type 316 stainless steel, with a diameter of 6 meters and a height of 22 meters. Additionally, 20 holding tanks (S-601, 602, 603, … 620) are used to store the liquid CO_2 following C-601 and are designed to hold one week's worth of production. Storage tanks will also be used to store MEA and MDEA on site before they are used in each amine scrubbing unit. A summary of storage tank design is given in

Table 4.9-3. Additionally, Two flash tanks are used in the second amine scrubbing unit for CO_2 removal that operate at a temperature of 40°C and 8 bar, and 45°C and 10 bar, respectively.

Table 4.9-3 Summary of storage tank design

Unit	Diameter (m)	Height (m)	Volume per Tank (m³)	Number
S-101 - S-120	20	32.6	10,242	20
S-121 - S-125	8	12.8	3,679	5
S-401 - S-405	18	23.5	5,986	10
S-501 - S-506	6	24.0	679	6
S-601 - S-620	16	18.3	3,681	20

5. Discussion
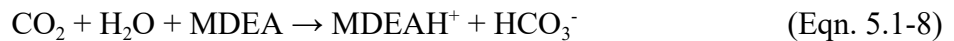
5.1 Amine Scrubbing for Hydrogen Sulfide Removal

Process Overview

The feed to this process is natural gas which is assumed to have a sour composition, meaning it contains relatively high amounts of hydrogen sulfide (H_2S) and carbon dioxide (CO_2). Once H_2S has been removed or minimized in the stream, the natural gas is referred to as "sweet gas." Hydrogen sulfide is a toxic gas and is harmful to the catalysts present in the reactors later in the process. Allowing it to remain in the process stream can poison the catalysts and quickly erode piping and equipment (*Amine Scrubbing System Overview*, n.d.). Therefore, removing it at the beginning will reduce maintenance costs in the long run. Additionally, H_2S is also extremely dangerous for humans and allowing it to continue through the process poses a safety hazard for operators and the community.

Solvent and Reactions

The removal of H_2S and CO_2 revolves around the use of amines that, in combination with water, serve to extract H_2S and CO_2 from the gas via a combination of dissociation and protonation reactions. The first step is the solubility of H_2S and CO_2 (Jassim, 2016). These initial steps allow the molecules to interact by bringing the H_2S and CO_2 into the liquid phase where their respective ions will be carried to the bottom of the absorber. H_2S is then separated into its ion form represented in Equations 1-4. Two dissociation reactions with H_2O breakdown H_2S in Equations 1 and 2 (Jassim, 2016). The tertiary amine, MDEA, also dissociates H_2S, but also competes with water for protonation of MDEA (Eqns. 2-4) (Jassim, 2016). In order to separate out carbon dioxide, CO_2 is converted to the bicarbonate in a series of three kinetic reactions with H_2O, OH^-, and MDEA (Eqns. 6-8) (Jassim, 2016). The bicarbonate is then dissociated further by H_2O in an equilibrium driven reaction (Eqn. 5).

$$H_2O + H_2S = H_3O^+ + HS^- \qquad \text{(Eqn. 5.1-1)}$$

$$H_2O + HS^- = H_3O^+ + S^{-2} \qquad \text{(Eqn. 5.1-2)}$$

$$MDEA + H_2O = OH^- + MDEA^+ \qquad \text{(Eqn. 5.1-3)}$$

$$H_2S + MDEA = MDEA^+ + HS^- \qquad \text{(Eqn. 5.1-4)}$$

$$HCO_3^- + OH = H_2O + CO_3^{2-} \qquad \text{(Eqn. 5.1-5)}$$

$$CO_2 + H_2O \rightarrow H^+ + HCO_3^- \qquad \text{(Eqn. 5.1-6)}$$

$$CO_2 + OH^- \rightarrow HCO_3^- \qquad \text{(Eqn. 5.1-7)}$$

$$CO_2 + H_2O + MDEA \rightarrow MDEAH^+ + HCO_3^- \qquad \text{(Eqn. 5.1-8)}$$

It is important to note that all reactions except those modeled by Equations 6-8 are equilibrium based while the latter are kinetic based. The thermodynamic model for this vapor-liquid equilibrium (VLE) system of H_2S-CO_2-MDEA-H_2O electrolytes was modeled in

Aspen Plus via its internal amine package. For this reason, MDEA instantly reacts with H_2S and then slowly reacts with CO_2 (Jassim, 2016). MDEA exhibits high selectivity towards H_2S, which is one of the reasons it was chosen as the primary solvent. While this means less CO_2 will be removed from the stream, it is the priority of this unit operation to eliminate H_2S from the system in order to ensure the safety of the operators and integrity of the process. Other advantages of MDEA include a low vapor pressure, low energy requirements, and high capacity and stability (Jassim, 2016). In addition, Aspen's ELECNRTL property method was used to model other ions in the system and Henry's Law was used to model the binary interactions of select ions.

Aspen Modeling
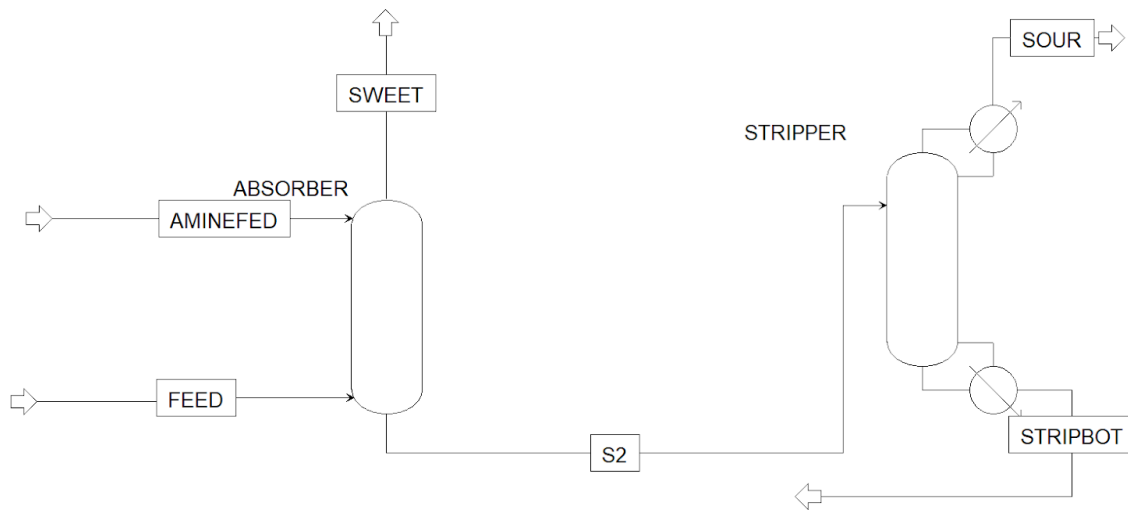
Figure 5.1-1 Aspen Plus model of first amine scrubbing unit

Table 5.5-1 provides a summary of the dimensions and parameters for both the absorber and stripper columns. Data for the columns were derived from "Sensitivity analyses and optimization of a gas sweetening plant for hydrogen sulfide and carbon dioxide capture using methyldiethanolamine solutions" by S. Jassim Majeed. Specifications such as inside diameter and tray spacing were taken from Aspen Plus which optimizes these parameters based on input

conditions provided. The stripper is temperature dominated, operating between 100.6-124.6°C with a bottoms pressure of 220 kPa, while the absorber is pressure dominated, operating between 57.8-73.1°C with a bottoms pressure of 2680 kPa. The recycle stream was not modeled in Aspen Plus and instead was calculated by hand by accounting for losses in the stripper and feeding those losses back into the absorber via a makeup stream. Though, a heater and pump were modeled in Aspen Plus from the stripper bottoms to account for this stream to be fed back into the absorber as a theoretical recycle stream. Since there is not a recycled stream modeled in Aspen Plus, there is no cross heat exchanger and instead there is simply a heating block that cools down the stream coming from the absorber to the stripper.

Table 5.1-1 Summary of absorber and stipper column dimensions and operating conditions

Parameter	Absorber	Stripper
Number of Stages	10	20
Inside Diameter (m)	2.01	1.40
Height of Main Section (m)	6.096	9.9
Tray Spacing (m)	0.610	0.550
Condenser Type	N/A	partial vapor
Reboiler	N/A	kettle
Tray Type	valve	valve
Feed Tray Number	1,10	3
Bottom Pressure (kPa)	2680	220
Pressure Drop (kPa)	60	20
Temperature Range (°C)	57.8 - 73.1	100.6 - 124.6

5.2 Autothermal Reformer

There are multiple routes available to convert methane (CH_4) into hydrogen (H_2), most of which require a great deal of energy input to the system. Our use of an autothermal reformer (ATR), however, utilizes the highly exothermic (ΔH = -802.7 kJ/mol) combustion of some of the feed methane to provide the energy required for subsequent reactions that produce hydrogen, thus lowering the energy costs associated with our plant (Halabi et al., 2008). The initial combustion of methane is shown below:

$$CH_4 + 2O_2 \rightarrow CO_2 + 2H_2O \qquad\qquad \text{(Eqn. 5.2-1)}$$

This reaction occurs very quickly, so in order to limit the combustion of methane, oxygen (O_2) is injected to the feed stream far below the stoichiometric requirement for total conversion. The partially reacted gasses then move down the column into the catalyst bed where three other reactions occur to produce hydrogen: steam methane reforming to carbon dioxide (CO_2), steam methane reforming to carbon monoxide (CO), and a water-gas shift (WGS) reaction. These reactions are described below, respectively:

$$CH_4 + 2H_2O \leftrightarrow CO_2 + 4H_2 \qquad\qquad \text{(Eqn. 5.2-2)}$$

$$CH_4 + H_2O \leftrightarrow CO + 3H_2 \qquad\qquad \text{(Eqn. 5.2-3)}$$

$$CO + H_2O \leftrightarrow CO_2 + H_2 \qquad\qquad \text{(Eqn. 5.2-4)}$$
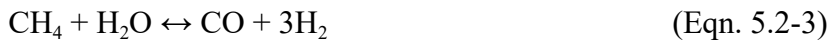
Both steam methane reforming reactions are endothermic (ΔH = 164.9 kJ/mol and ΔH = 206.2 kJ/mol, respectively) whereas the final water-gas shift reaction is slightly exothermic (ΔH = -41.1 kJ/mol) (Halabi et al., 2008). Table 5.2-1 provides the temperature dependent rates used to model each reaction occurring in the ATR with p_j corresponding to the partial pressure of component j in units of bar, along with the reaction's respective kinetic parameters (Hoang & Chan, 2004).

Table 5.2-1. Reaction rates and kinetic parameters for the ATR

Rxn (i)	Rate (mol/kg$_{cat}$-s)	k_{oi} (mol/kg$_{cat}$-s)	E_i (kJ/mol)
(1)	$\dfrac{k_1 p_{CH_4} p_{O_2}^{0.5}}{\left(1 + K_{CH_4}^C p_{CH_4} + K_{O_2}^C p_{O_2}^{0.5}\right)^2}$	5.852e+17 bar$^{-1.5}$	86.00
(2)	$\dfrac{\dfrac{k_2}{p_{H_2}^{2.5}}\left(p_{CH_4} p_{H_2O} - \dfrac{p_{H_2}^3 p_{CO}}{K_{e2}}\right)}{\left(1 + K_{CO} p_{CO} + K_{H_2} p_{H_2} + K_{CH_4} p_{CH_4} + \dfrac{K_{H_2O} p_{H_2O}}{p_{H_2}}\right)^2}$	4.225e+15 bar$^{0.5}$	240.1
(3)	$\dfrac{\dfrac{k_3}{p_{H_2}^{3.5}}\left(p_{CH_4} p_{H_2O}^2 - \dfrac{p_{H_2}^4 p_{CO_2}}{K_{e3}}\right)}{\left(1 + K_{CO} p_{CO} + K_{H_2} p_{H_2} + K_{CH_4} p_{CH_4} + \dfrac{K_{H_2O} p_{H_2O}}{p_{H_2}}\right)^2}$	1.020e+15 bar$^{0.5}$	243.9
(4)	$\dfrac{\dfrac{k_4}{p_{H_2}}\left(p_{CO} p_{H_2O} - \dfrac{p_{H_2} p_{CO_2}}{K_{e4}}\right)}{\left(1 + K_{CO} p_{CO} + K_{H_2} p_{H_2} + K_{CH_4} p_{CH_4} + \dfrac{K_{H_2O} p_{H_2O}}{p_{H_2}}\right)^2}$	1.955e+06 bar^{-1}	67.13

$$k_i = k_{oi} \, exp\left(\frac{-E_i}{RT}\right)$$
(Eqn. 5.2-5)

The kinetic parameters k_i are calculated using Equation 5.2-5 where E_i is the activation energy of reaction i in kJ/mol, R is the gas constant in kJ/mol-K, and T is the reactor temperature in K. Furthermore, equilibrium constants K_{ei} and adsorption components K_{oj} (pre-exponential factors) and H_j (heats of adsorption) are provided in Tables 5.2-2 and 5.2-3, respectively, with K_j calculated using equation 5.2-6 (Luneau et al., 2017).

$$K_j = K_{oj} \, exp\left(\frac{-H_j}{RT}\right)$$
(Eqn. 5.2-6)

Table 5.2-2. Values of equilibrium constants for reactions 2-4

Equilibrium constant	Value
K_{e2}	$exp(-26830/T + 30.114)$ bar^2
K_{e3}	$K_{e2} K_{e4}$ bar^2
K_{e4}	$exp(4400/T - 4.036)$

Table 5.2-3. Adsorption equilibrium constants for reactions 1-4

Adsorption Equilibrium Constant	K_{oj}	H_j (kJ/mol)
K_{CH_4}	6.64e-04 bar^{-1}	-38.3
K_{CO}	8.23e-05 bar^{-1}	-70.7
K_{H_2}	6.12e-09 bar^{-1}	-82.9
K_{H_2O}	1.77e+05	+88.7
$K_{CH_4}^{C}$	1.26e-01 bar^{-1}	-27.3
$K_{O_2}^{C}$	7.78e-07 bar^{-1}	-92.8

This reactor starts at a pressure of 30 bar and temperature of around 900°C, falling to about 29.5 bar and 680°C by the bottom of the column, as calculated by Aspen. In order to reach this temperature after start-up, the initial oxygen feed is increased to match the inlet methane flow in a 1:1 molar ratio until the reactor's temperature rises to the desired level, at which point oxygen flow is reduced to operating input. The reactor then maintains its temperature by balancing the heat produced via the combustion of methane and WGS reactions with the heat absorbed by the two steam methane reforming reactions.

Catalyst

The ATR is fully packed with catalyst; therefore, each reaction taking place is dependent upon the gas adsorption into the catalysts, accounted for via the denominator of each rate equation. The catalyst used in this reactor, Ni/MgAl$_2$O$_4$, was first studied with regards to methane reforming by Xu and Froment (1989) to develop the rate equations shown above. It consists of 15.2% nickel supported on a magnesium aluminate spinel which is crushed into particles of diameter 0.18-0.22 mm. Within the column, the catalyst density is 1870 kg/m^3 and the catalyst bed has a void fraction of 0.528.

Aspen Modeling

In order to model this reactor in Aspen Plus, three separate RPlug reactors were used to imitate the four stages of reactions occurring in the reactor: total combustion followed by the CO generating steam methane reforming reaction, the WGS reaction, and finally the CO_2 generating SMR reaction, using the kinetic models described above. Though each of these reactions are occuring within the same space, modeling these sections separately allows for a more streamlined depiction of the reactions at different points along the reactor. Furthermore, the Peng-Robinson equation of state was used in this model as was suggested by the literature sources from which the kinetic data was retrieved, and due to its adequate modeling of natural gas properties and reactions. In order to ensure that the reactor is autothermal, the heat duties of each of the three reactors are summed to 0, thus assuming a fully isothermal reactor. The Aspen model used for this system is given in Figure 5.2-1.
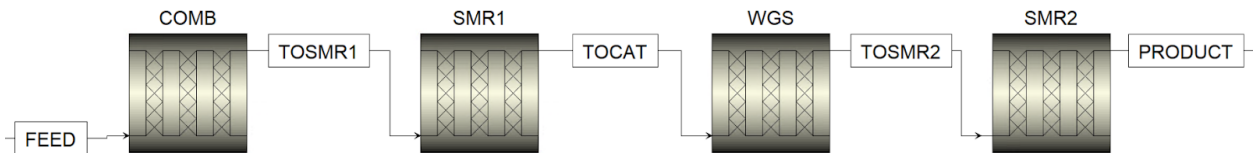
Figure 5.2-1. Aspen model of the ATR split into four separate reactors

In modeling this unit, the reactor dimensions were designated as 28.5 m in height and 4 m in diameter with the combustion section modeled as 0.5 m, the first reforming section as 20 m, the WGS section as 4 m, and the second reforming section as 4 m. Under these conditions, an 85% CH_4 conversion is reached producing an output of 2.2 mol% CH_4, 45 mol% H_2, and 11 mol% CO along with some CO_2, nitrogen (N_2), and water (H_2O). This output stream flows directly from the bottom of the ATR through a cooler before entering the first of two WGS reactors.

5.3 Water-Gas Shift Reactors

In order to reduce the amount of CO and increase the amount of H_2 in the syngas, the stream leaving the ATR is sent to a series of water-gas shift (WGS) reactors. The primary reaction occurring in these reactors is the same WGS reaction that occurs in the ATR and is listed again below:

$$CO + H_2O \leftrightarrow CO_2 + H_2 \qquad \text{(Eqn. 5.3-1)}$$

This reaction is exothermic (ΔH = -41.1 kJ/mol) and reversible and is thus thermodynamically favored at low temperatures, but kinetically favored at high temperatures. Due to these limitations, industrial water-gas shift systems typically occur in two stages — a high temperature (HT) reactor and a low temperature (LT) reactor — to maximize CO conversion (Mendes et al., 2009). The reaction is commonly modeling using a power-law based rate expression shown below:

$$r = k_0 exp(-\frac{E}{RT})P_{CO}^n P_{H_2O}^m P_{CO}^p P_{H_2}^q (1 - \frac{P_{CO_2} P_{H_2}}{P_{CO} P_{H_2O} K_{eq}}) \qquad \text{(Eqn. 5.3-2)}$$

In this rate expression, r represents reaction rate in mol/g_{cat}-s, k_0 is a pre-exponential factor, E_a is the activation energy in kJ/mol, R is the universal gas constant, T is absolute temperature in Kelvin, K_{eq} is the reaction equilibrium constant, P is the partial pressure of reaction component i in kPa, and the exponents n, m, p, and q are parameters estimated from experimental data. The term in parentheses at the end of the expression is considered the approach to equilibrium and accounts for the reversibility of this reaction (Hla et al., 2009).The equilibrium constant, K_{eq}, is defined by the expression below:

$$K_{eq} = exp(\frac{4577.8}{T} - 4.33) \qquad \text{(Eqn. 5.3-3)}$$

Catalysts

The reaction was modeled in catalytic packed bed reactors, consistent with literature. For the HT reactor, an iron-chromium based catalyst was used, as they are common industrial HT catalysts due to their improved selectivity and catalytic performance (Mendes et al., 2009). The specific catalyst chosen is composed of 87% Fe_2O_3 , 11% Cr_2O_3 , and 2% CuO, has a particle diameter of 6 mm, and a calculated density of 5256 kg/m^3 (Hla et al., 2009). The kinetic parameters specific to this catalyst are given in Table 5.3-1 (Adams & Barton, 2009). Additionally, the equilibrium constant for a reactor temperature of 400°C was calculated to be 11.8.

For the LT reactor, a copper-zinc based catalyst was chosen because they are widely used to achieve higher conversions at low temperatures, but exhibit thermal instability at high temperatures (Mendes et al., 2009). The specific catalyst chosen is composed of 24.9% CuO, 43.7% ZnO, and 31.4% Al_2O_3 and has a calculated density of 5256 kg/m^3 (Ayastuy et al., 2004). Additionally, a particle diameter of 6 mm was chosen to remain consistent with the HT reactor. The kinetic parameters specific to this catalyst are given in Table 5.3-1 (Ayastuy et al., 2004). Additionally, the equilibrium constant for a reactor temperature of 175°C was calculated to be 361.

Table 5.3-1. Kinetic parameters for HT and LT catalysts

Catalyst	k_0	E_a	m	n	p	q
HT	725 mol/g$_{cat}$-s-kPa	110 kJ/mol	1	0	-0.32	-0.083
LT	63660 mol/g$_{cat}$-s-kPa	79.7 kJ/mol	0.47	0.72	-0.65	-0.38

Aspen Modeling

An RPlug reactor was used to model this system in Aspen Plus in order to appropriately model the catalyst loading and associated kinetics of the reaction. The Peng-Robinson property

method was used because the process stream consists of largely nonpolar compounds, including hydrocarbons and light gasses and is a recommended property method for gas processing. Reaction kinetics were entered using a custom reaction class and the parameters defined above. The Aspen Plus model of the two reactor system is given in Figure 5.3-1. The reactors were modeled as catalytic-packed bed reactors consisting of multiple reactor tubes within a thermal fluid shell. A shell and tube reactor design was chosen due to the large heat transfer requirements of the exothermic reaction to maintain isothermal operation in the reactor.
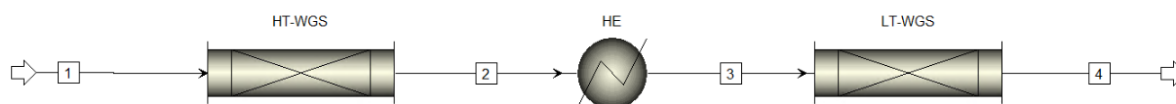
Figure 5.3-1. Aspen Plus model of the two water-gas shift reactor system

For the HT reaction, a temperature of 400°C was chosen within the range of typical HT reactor operation (Chen & Chen, 2020). A sensitivity analysis revealed that temperatures up until 430°C resulted in higher conversion of CO, but with diminishing returns and were unnecessary. A pressure of 30 bar was chosen for the HT reactor, as this was the pressure of the process stream leaving the reformer, reducing the need for additional compressors. An Aspen simulation calculated a pressure drop of 3.79 bar using the Ergun equation, with the process stream leaving at a pressure of about 26 bar. The heat duty of the reactor was -36.9 MW. Water was used in the shell of the reactor to remove excess heat produced, entering at 80°C and a flow rate of 60,000 kg/hr and leaving as steam at the same temperature and flow rate. These were the temperature and flow rate necessary to maintain isothermal conditions in the reactor according to the Aspen model. These conditions resulted in a 92.5% conversion of CO and 33.7% conversion of H_2O.

For the LT reactor, a temperature of 175°C was chosen within the range of typical LT reactor operation (Chen & Chen, 2020). A heat exchanger between the reactors was used to cool the process stream to 175°C before entering the reactor. A pressure of 26 bar was chosen for the LT reactor, again to use the existing stream pressure and avoid requiring an additional compressor. The calculated pressure drop for this reactor was 2.75 bar and the heat duty was determined to be -2.54 MW. Water was once again used in the shell of the reactor to remove excess heat produced and entered at 155°C at a flow rate of 25,000 kg/hr and left as steam at the same temperature and flow rate. Again, these were the temperature and flow rate necessary to maintain isothermal conditions in the reactor according to the Aspen model. Steam produced in both reactor shells will be sold to reduce utility costs.The CO conversion in the LT reactor was 100%, resulting in an overall CO conversion for the system of 100%. For H_2O, conversion in the LT reactor was 0.04%, resulting in an overall system conversion of 36.4% A summary of operating conditions for each reactor is given in Table 5.3-2.

Table 5.3-2. Operating conditions and conversions of both reactors

Condition	HT Reactor	LT Reactor
Temperature (°C)	400	175
Pressure (bar)	30	26
Pressure Drop (bar)	3.79	2.75
Heat Duty (MW)	-36.9	-2.54

Reactor Dimensions

Dimensions were kept constant between both reactors for consistency and ease of design. A tube diameter of 0.1 m was chosen as the maximum diameter that could be used before heat transfer issues occurred within the tubes. The Aspen optimization tool was used to determine the length of pipe and number of tubes that maximized conversion while reducing pressure drop,

resulting in a tube length of 1.5 m and 750 tubes. Using a correlation provided by Benyahia & O'Neill (2005) between the tube diameter, catalyst particle diameter, and bed voidage, the bed void fraction was determined to be 0.38. Using the catalyst density and total reactor volume, the total catalyst loading was calculated to be about 28,800 kg for the HT reactor and 30,500 kg for the LT reactor. The chosen material of construction for this reactor is stainless steel because it's corrosion resistant, durable, and relatively cost effective (*Duplex stainless steel reactors,* 2021). A summary of reactor dimensions and specifications is given in Table 5.3-3.

Table 5.3-3. Reactor dimensions and specifications for each reactor

Parameters	HT Reactor	LT Reactor
Tube Diameter (m)	0.1	0.1
Tube Length (m)	1.5	1.5
Number of Tubes	750	750
Particle Diameter (mm)	6	6
Bed Voidage	0.38	0.38
Catalyst Loading (kg)	28,800	30,500

5.4 Amine Scrubbing for Carbon Dioxide Separation

Following the WGS reactors where the syngas feed is shifted, a second amine scrubber is used to separate CO_2 from the product stream. Absorption is a tried and proven method for CO_2 separation at a commercial scale, with initial designs being published back in the 1930s (Rochelle, 2009). This process works the same as AS1: a compound in the feed, in this case CO_2, is absorbed into a solvent where it is then stripped out and recovered without the other components.

Solvent and Reactions

Choosing an ideal solvent for amine scrubbing units can be challenging, as one must balance both biodegradability of the solvent and its stability. Low biodegradable solvents can pose significant problems for the environment, while a lack of stability can hinder the plant's operation, both of which affect individuals' health and safety (Capello et al., 2007). Monoethanolamine (MEA), a volatile organic compound that contains both a primary amine and primary alcohol, was chosen due to its high biodegradability and moderate stability at process conditions (Eide-Haugmo et al., 2011). It also has a significant reputation as a CO_2 capture solvent, as it has been successfully used in multiple plants around the world for decades (Chai, 2022). When using MEA for CO_2 capture, the key reactions to be aware of are the formation of bicarbonate and carbamate. These are represented by Equations 1 and 2, both of which occur in the absorber (Pinsent et al., 1956). The reverse of these reactions, when bicarbonate and carbamate are split back up into their components, are represented by Equations 3 and 4 (Hikita et al., 1997). Heat and pressure promote these decomposition reactions, which occur in the stripper column.

$$CO_2 + OH^- \rightarrow HCO_3^- \qquad\qquad\qquad \text{(Eqn. 5.4-1)}$$

$$MEA + CO_2 + H_2O \rightarrow MEACOO^- + H_3O^+ \qquad\qquad \text{(Eqn. 5.4-2)}$$

$$HCO_3^- \rightarrow CO_2 + OH^- \qquad\qquad\qquad \text{(Eqn. 5.4-3)}$$

$$MEACOO^- + H_3O^+ \rightarrow MEA + CO_2 + H_2O \qquad\qquad \text{(Eqn. 5.4-4)}$$
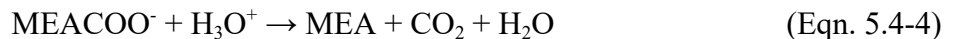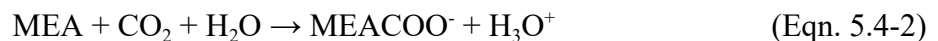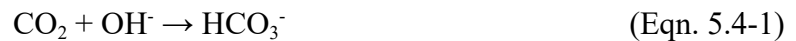
Reaction rates for Equations 5.4-1 - 5.4-4 are given in Equations 5.4-5 - 5.4-8, where it should be noted that the rate constant for the first reaction is equal to the rate constant of the fourth reaction (Pinsent et al., 1956; Hikita et al., 1997). The same can be said for the rate constants of the second and third reactions.

$$r_1 = k_1 a_{CO_2} a_{OH^-} \qquad \text{(Eqn. 5.4-5)}$$

$$r_2 = k_2 a_{MEA} a_{CO_2} \qquad \text{(Eqn. 5.4-6)}$$

$$r_3 = \frac{k_1}{K_{HCO_3^-}} a_{HCO_3^-} \qquad \text{(Eqn. 5.4-7)}$$

$$r_4 = \frac{k_2}{K_{MEACOO^-}} \times \frac{a_{MEACOO^-} * a_{H_3O^+}}{a_{H_2O}} \qquad \text{(Eqn. 5.4-8)}$$

Equilibrium reactions for AS2 include water dissociation, CO_2 hydrolysis, bicarbonate dissociation, carbamate hydrolysis, and MEA protonation (Zhang, 2013). These reactions, in conjunction with the bicarbonate and carbamate formation reactions, form the chemistry basis of this process unit.

Aspen Modeling and Resultant Dimensions

The design of this amine scrubber was based on the design of Lange et al. (2020), a UVA chemical engineering capstone group whose project involved carbon capture, storage, and utilization. In order to model this amine scrubber in Aspen Plus, RadFrac blocks were used to model the absorber and stripper columns, with flash and heater blocks used to model the flash drums and heat exchangers, respectively. To account for the ions involved in this process, Electrolyte Wizard was used to determine generated ions and ENRTL-SR was chosen as the property method due to its ability to model electrolyte systems with unsymmetric reference states for ionic species . Although reaction kinetics are known for the bicarbonate and carbamate reactions, they were not used explicitly in the design of the absorber or stripper. Packed columns of generic metal pall rings were utilized for both the absorber and the stripper. The Aspen model for AS2 is given in Figure 5.4-1.
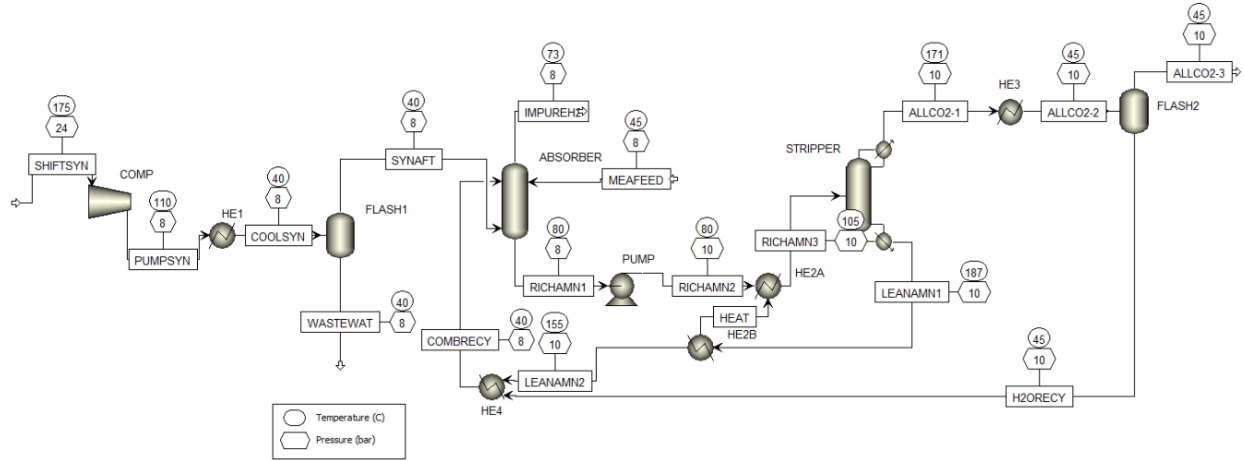
Figure 5.4-1 - Aspen Plus model of the second amine scrubber

For the absorber, four theoretical packed stages consisting of ⅝" generic metal pall rings were specified, each at an equivalent packing height (HETP) of 3.33 meters. This HETP was chosen based on the research gathered from Afkhamipour & Mofarahi (2017), where optimal absorption columns using MEA to separate CO_2 had HETPs of approximately 1-6.55 meters. Lange et al. (2020) utilized an HETP of 3.33 meters, so this value was taken directly from them, leading to a total column height of 13.32 meters. Pall rings were chosen over berl saddles for packing material because they could better stabilize column operating conditions. A column pressure of 8 bar was specified to improve overall separation and decrease column size, both of which help with the economic feasibility of this project. Feed streams were specified such that they were consistent with proper absorption column operation (Price, 2022). The diameter of the column was determined by Aspen Plus to be 9.82 meters, given our specifications and operating parameters, which also resulted in a pressure drop of 0.0631 bar. Distillate and bottoms streams, as well as their compositions and temperatures were also determined by Aspen Plus. A summary of the absorber dimensions and design specifications can be found in Table 5.4-1.

Table 5.4-1 Absorber dimensions and design specifications summary

|	
Avg Temperature (°C)	80.3
Pressure (bar)	8.00
Pressure Drop (bar)	0.0631
Diameter (m)	9.82
Number of Packed Stages	4
HETP (m)	3.33
Packing Type	⅝" Generic Metal Pall Rings

For the stripper column, seven theoretical packed stages consisting of 3.5" generic metal pall rings were specified, each at an HETP of 2.83 meters. The HETP was chosen based on the stripper column designed by Lange et al. (2020), which itself was based on research for optimal stripper HETPs from Garcia et al. (2017). Pall rings were chosen over berl saddles for the same reason as the absorber column: better stabilization of column operating conditions. Pressure for the stripper column was specified at 10 bar, also to decrease overall column size and improve separation. A reflux ratio of 0.5 and bottoms rate of 3.4 million kg/hr were also specified. After running the simulation, Aspen Plus calculated the diameter of the column to be 10.7 meters, with a pressure drop of 0.0885 bar. It also determined the heat duties of the reboiler and condenser at 1030 and -205 MW respectively. A summary of the stripper dimensions and design specifications can be found in Table 5.4-2.

Table 5.4-2 - Stripper Dimensions and Design Specifications Summary

Avg Temperature (°C)	182
Pressure (bar)	10.0
Pressure Drop (bar)	0.0885
Diameter (m)	10.7
# of Packed Stages	7
HETP (m)	3.20
Packing Type	3.5" Generic Metal Pall Rings
Heat Duty - Reboiler (MW)	1030
Heat Duty - Condenser (MW)	-205

5.5 Pressure Swing Adsorption

After removing most of the CO_2 through AS2, the hydrogen product must be further purified to 99.99% H_2 to be viable for sale. Pressure swing adsorption (PSA) is used to achieve this purity due to its relatively safe operating conditions, moderately high recovery, and scalability. PSA separates impurities and products by using differences in binding affinity to an adsorbent material. These differences, along with adsorption capacity, can increase with increasing pressure as shown in Figure 5.5-1.
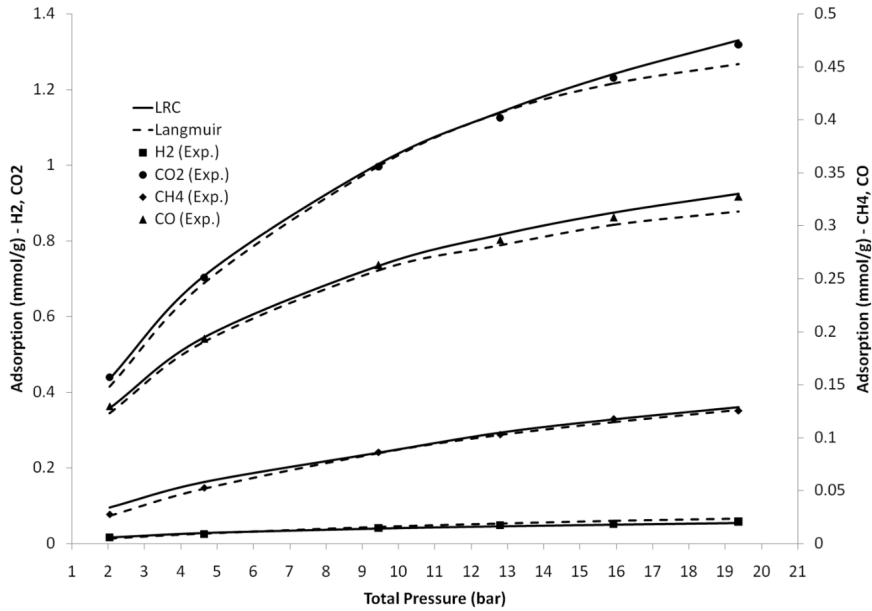
Figure 5.5-1 Equilibrium isotherms and amount of gas adsorbed on zeolite 5A at 45°C

(Yavary et al., 2016)

Figure 5.5-1 provides adsorption data for components relevant to H_2 purification with respect to pressure on zeolite 5A, a common commercial PSA adsorbent. According to this data, adsorption of impurities like CO, CH_4, and CO_2 increases more rapidly than H_2 with increasing pressure. PSA takes advantage of this by increasing pressure to increase adsorption of impurities, extracting the product (mostly remaining H_2 in bulk gas), and decreasing pressure to desorb impurities from the adsorbent materials and send them to the waste stream, also called tail gas.

Design

The general concept of PSA can be applied to create a multi-bed cycle process to increase the utility of high pressure gas within the system and to increase overall capacity. The design for our PSA unit is based on US Patent 6,340,382 (Baksch & Ackley, 2002). The patent has a similar PSA feed composition to our process, as shown in Table 5.5-1, albeit we have a much higher H_2 presence which will ensure product purity. The decreased CO_2 presence in our design could

potentially benefit from a decreased use in activated carbon in favor of zeolites, but this will be discussed further in the *Adsorbents* section.

Table 5.5-1 Comparison of PSA feed compositions in patent and project design

Component	Patent Feed Composition (mol%)	PSA Feed Composition (mol%)
H_2	0.74	0.92
CH_4	0.02	0.04
CO	0.01	0.00
CO_2	0.22	0.01
N_2	0.01	0.02
H_2O	0.00	0.01

Bed sizing was calculated based on size factors provided in the patent, displayed in Table 5.5-2. These indicate the amount of packing required for a specified H_2 production rate in tons per day (TPD).

Table 5.5-2 Size Factors for PSA Packing

Adsorbent	Size Factor (kg/TPD H_2)
Alumina	470.98
Activated Carbon	2229.93
Zeolite	684.90
Overall	3385.80

Table 5.5-3 outlines the process conditions for the unit, where P_{ad} and P_{de} are the adsorption and desorption pressures, respectively. Pressure drop for these beds was determined to be negligible, based on long step times and pressure being changed in gradual stages as opposed to a flash.

Table 5.5-3 Process conditions for PSA unit

Cycle time (s)	600
Tons per day (TPD) H_2	750
Temperature (K)	311
P_{ad} (bar)	11.71
P_{de} (bar)	1.33
Feed Flow (kg/hr)	77,000
H_2 Purity	0.99993
H_2 Recovery	0.816

Note that while product purity leaving this unit is excellent, an 81.6% overall recovery in

a commodity chemical process is undesirable, and the tail gas stream is still about 50 mol% H_2.

Future work should consider installing additional four-bed units to process the tail gas stream

and recover additional hydrogen.

Operations

This unit will operate on a 12-step cycle, designed to allow for adsorption steps to occur

for 25% of the total cycle time. Table 5.5-4 describes what occurs during each step. Note that in

EQ steps, beds are equalizing with each other. This improves efficiency by removing the need for

additional compression after adsorption is complete, and decreases the overall energy

requirement of the unit. Multiple adsorption steps are also used to the same effect, with the bed

closed off to others in AD1, and then using that pressure to increase product pressure gradually

to another bed during AD2 and AD3. To get an overall sense of how the beds work together,

Table 5.5-5 outlines the overall cycle for each four-bed system, including what step each bed is

in during the cycle and step times. Note that the initial adsorption time (AD1) is always 40 s,

while final product pressurization (PP2) takes the shortest time (25 s), and purge steps take the longest (85 s).

Table 5.5-4 Step-by-step description of PSA cycle

| Step	Action
AD1 (Adsorption 1)	Receiving feed at adsorption pressure
AD2 (Adsorption 2)	PP1 to another bed
AD3 (Adsorption 3)	PP2 to the same bed as PP1
EQ1DN (Equalizing Down 1)	Decreasing pressure, providing high pressure gas to another bed for EQ2UP
PPG (Providing Purge Gas)	Providing purge gas to another bed
EQ2DN (Equalizing Down 2)	Decreasing pressure, providing low pressure gas to another bed for EQ1UP
BD (Blowdown)	Countercurrent blowdown
PG (Purge)	Receiving purge gas, to tail gas stream
EQ1UP (Equalizing Up 1)	Increasing pressure, receiving low pressure gas from another bed in EQ2DN
EQ2UP (Equalizing Up 2)	Increasing pressure, receiving high pressure gas from another bed in EQ1DN
PP1 (Product Pressurization 1)	Product pressurization from AD2
PP2 (Product Pressurization 2)	Product pressurization from AD3, to product stream

Table 5.5-5 - Overall PSA cycle for a four-bed system

Step	Bed 1 (B1)	Bed 2 (B2)	Bed 3 (B3)	Bed 4 (B4)	Step Time (s)
1	AD1	BD	EQ1DN to B4	EQ2UP from B3	40
2	AD2, PP1 to B4	PG from B3	PPG to B2	PP1 from B1	85
3	AD3, PP2 to B4	EQ1UP from B3	EQ2DN to B2	PP2 from B1	25
4	EQ1DN to B2	EQ2UP from B1	BD	AD1	40
5	PPG to B3	PP1 from B4	PG from B1	AD2, PP1 to B2	85
6	EQ2DN to B3	PP2 from B4	EQ1UP from B1	AD3, PP2 to B2	25
7	BD	AD1	EQ2UP from B4	EQ1DN to B3	40
8	PG from B4	AD2, PP1 to B3	PP1 from B2	PPG to B1	85
9	EQ1UP from B4	AD3, PP2 to B3	PP2 from B2	EQ2DN to B1	25
10	EQ2UP from B2	EQ1DN to B1	AD1	BD	40
11	PP1 from B3	PPG to B4	AD2, PP1 to B1	PG from B2	85
12	PP2 from B3	EQ2DN to B4	AD3, PP2 to B1	EQ1UP from B2	25

Adsorbents

In PSA, it is common to use several layers of adsorbent materials within each bed, each with an affinity for a particular impurity. This process will use three adsorbents: CaX zeolite, activated carbon, and alumina. Alumina is primarily used for the removal of residual H_2O in the stream. The adsorbent is thermally and mechanically resistant, does not corrode, and is active enough to adsorb water vapor out of air at ambient temperature (Dynamic Adsorbents, n.d.). Only 6% of packing will consist of alumina due to the low water content in the feed, as most will be condensed out of the feed stream. .

Activated carbon is used to selectively adsorb CO, CO_2, and CH_4, and its affinity for these impurities is shown in Figure 5.5-3.
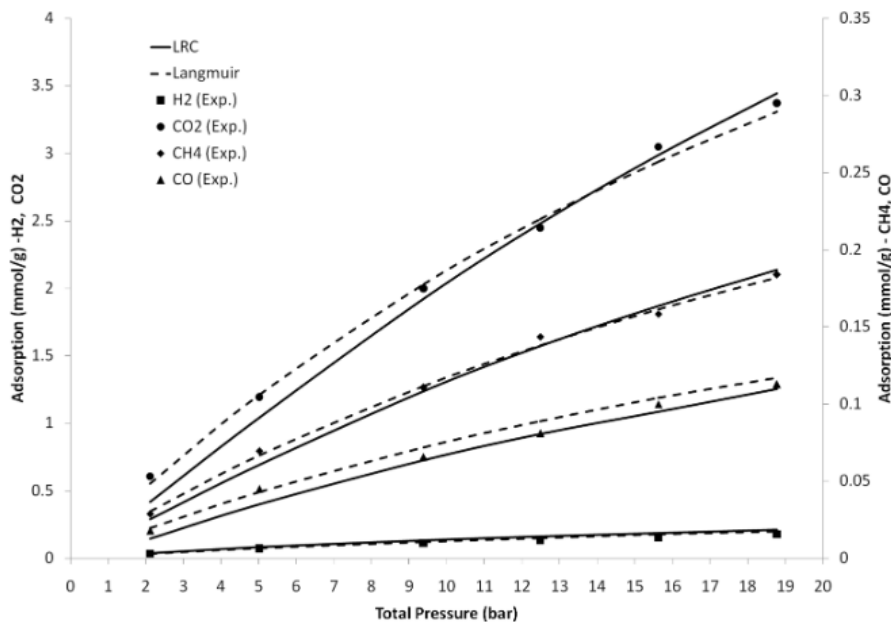
Figure 5.5-3 Adsorption data for H_2 and impurities on activated carbon at 45°C

(Yavary et al., 2016)

According to this data, CO_2 has a strong affinity for activated carbon, but there is good separation present between all impurities. H_2 also has a very weak affinity for the adsorbent, allowing product to flow through the next layer. Since CH_4 is a significant impurity in the feed, about 53% of packing volume will be activated carbon. With future testing this could potentially be decreased to accommodate for the decreased CO_2 presence in the feed, but product purity is a top priority.

The final layer of packing consists of CaX zeolite, also known as "molecular sieve". With a pore size of 4.8 Å, the material slows down larger molecules while letting smaller molecules like H_2 pass through more quickly (Li et al., 2020). This layer is used to remove remaining impurities that activated carbon and alumina could not capture, and is selective enough to separate H_2 and N_2. The adsorption isotherm of this material is displayed in Figure 5.5-1, in the beginning of the PSA section.

Packing composition was calculated based on size factors displayed in Table 5.5-2. The packing configuration for each bed is displayed in Figure 5.5-4.
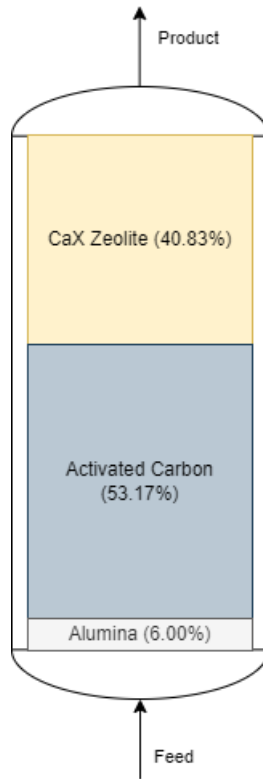
Figure 5.5-4 Packing composition and arrangement for PSA beds

The arrangement of the packing was chosen so that the pore size decreases as the gas moves up the column. This reduces adsorption step time by increasing the contact time of the feed through all layers, allowing quick passage of product through alumina and activated carbon compared to zeolite.
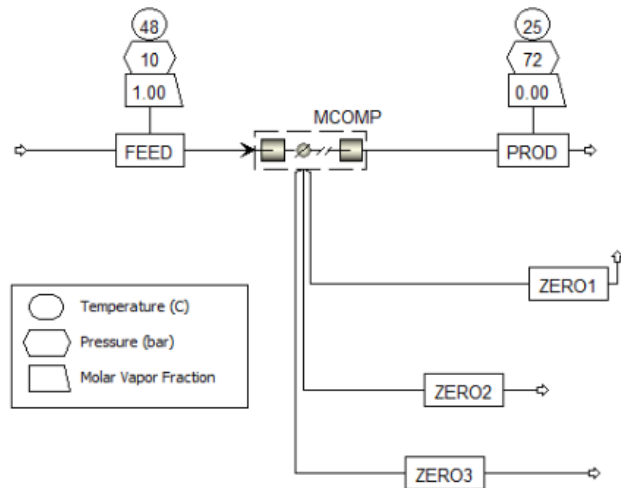
5.6 Carbon Dioxide Compression

In order to sell the captured CO_2 for enhanced oil recovery (EOR), the CO_2 must be liquified for transportation and future treatment at the EOR site. According to Professor Anderson, companies who engage in EOR prefer the CO_2 to be at room temperature (25°C).

Therefore, in consultation with a phase diagram for CO_2, the gaseous product stream must be compressed to some pressure between 60 and 80 bar. A four-stage centrifugal compressor utilizing four heat exchangers will be used to meet these requirements.

Aspen Modeling

To model the four-stage compressor unit, an MCompr block was used with a specified outlet temperature and pressure of 25°C and 72.3 bar. Peng-Robinson was chosen as the property method due to the prevalence of nonpolar compounds in the stream, and because of its usage in every other unit operation that does not handle ions. Outlet pressure was determined by trial and error, where the lowest pressure resulting in a product stream liquid fraction of 1 was chosen. The feed stream was specified with the exact stream composition, flow, and pressure from AS2's CO_2 product stream (stream 39). However, a small but notable difference is the temperature of the feed stream. Due to the difference in property method used between AS2 and CO_2 Compression simulations, a different temperature is given from Aspen Plus after specifying a vapor fraction of one. Hence, there is a 3.1°C increase in temperature from AS2's product stream to CO_2 Compression's feed stream, with that feed stream's temperature being 48.1°C. The Aspen model for CO_2 Compression can be seen in Figure 5.6-1. Streams ZERO1, ZERO2, and ZERO3 have flow rates of 0 kg/hr and were only added because Aspen Plus required it.

Figure 5.6-1 Aspen Plus model for carbon dioxide compression unit

5.7 Ancillary Equipment

Heat Exchangers

A table summarizing the operating conditions for all 12 heat exchangers in this process can be found in section 4.9 Ancillary Equipment. Each of these units is designed as a shell and tube heat exchanger, as they are one of the most common designs for heat exchangers in chemical processing. Flow was assumed to be countercurrent, with the process stream flowing through the tube side and water flowing through the shell side, according to heuristics provided by Peters et al. (2003). Type 316 stainless steel was chosen as the material of construction due to its durability and resistance to corrosion, especially to hydrogen embrittlement which could become a problem with large amounts of hydrogen flowing through our system (San Marchi, 2005).

Equations 5.7-1 and 5.7-2 were used in the design of these heat exchangers and Aspen Plus was used to confirm and model these designs. Overall heat transfer coefficients, U_0, were assumed according to heuristics outlined by Peters et al. (2003): 850 W/m^{2}K for exchangers with phase changes, 285 W/m^{2}K for liquid-liquid exchangers, and 30 W/m^{2}K for all other exchangers

(Peters et al., 2003). For E-401, a value of 510 W/m^{2}K was used due to the hybrid nature of this heat exchanger (Lange et al., 2020).

$$Q \; = \; U_0 A \Delta T_{lm}$$ Eqn. 5.7-1

$$\Delta T_{lm} \; = \; \frac{(T_{H1}-T_{C1})-(T_{H2}-T_{C2})}{LN((T_{H1}-T_{C1})/(T_{H2}-T_{C2}))}$$ Eqn. 5.7-2

Steam produced in any of these heat exchangers will be sold to offset the utility costs for this operation. Heat integration strategies have not been implemented at this time, and is an area of work that future designs should explore.

Pumps and Compressors

Centrifugal compressors are chosen for this process due to their ability to handle large volumes of gas and bring them to moderate pressures. Unreliability is an important factor to consider, and redundant compressors and pumps along with regular maintenance will be required to maintain process operability.

Tanks

Holding tanks are implemented after PSA compression, and are designed to hold one cycle of capacity for the unit (~4100 m^3). This is to improve safety and reduce waste in the event of a PSA bed becoming ineffective for a time. These tanks are cylindrical and are made of type 316 stainless steel. Storage tanks for natural gas were sized to accommodate one hour's worth of feed and is to be supplied via pipeline, while both amine solvent storage tanks were sized to store six months worth of supply. CO_2 holding tanks were designed to hold one week's worth of product before being shipped via tanker trucks.

6. Economic Analysis

6.1 Capital Costs

The total capital cost for this proposed plant is based largely on the total equipment costs, along with the piping, installation, site development, electrical, contingency and legal fees associated with its construction. Equipment costs were estimated using CAPCOST, a cost estimation Excel software program from Turton et al. (2012). The software data was based on 2017 prices, so in order to account for inflation prices were escalated using the Chemical Engineering Plant Cost Index (CEPCI). The most recently available CEPCI for May 2022 of 831.1 was used in the program calculations ("Economic Indicators," 2022). For equipment sizing that exceeded the capacity of the program, costs were scaled up using the sixth-tenths rule for scaling cost estimates, given in Equation 6.1-1 (Turton et al., 2012).

$$C_a = C_b (\frac{A_a}{C_b})^{0.6} \qquad \text{Eqn. 6.1-1}$$

The bare module cost for each piece of equipment was chosen because it includes not only the equipment costs, but also the costs associated with materials, labor, freight and shipping, overhead, and engineering supervision (Turton et al., 2012). This provides a more holistic approach to capital cost estimation. The costs of catalysts and adsorbent beds were priced separately using vendor data and added on to the bare module costs for each piece of equipment where necessary. To compute the complete estimated capital cost, the total grassroots module cost provided by CAPCOST was used. This value includes the total bare module costs for all equipment, as well as contingency, fees, and site development costs to give a total estimate for the cost of plant equipment and construction. This was estimated by CAPCOST to be almost $820 million. Working capital for the plant was assumed to be 15% of the total grassroots

module cost at about $93.6 million. Combined, the total capital investment of this plant is estimated to be roughly $912 million. Tables 6.1-1 through 6.1-3 provide the bare module costs for all major equipment, heat exchangers, pumps and compressors and Table 6.1-4 provides a summary of the total capital cost of this plant.

Table 6.1-1 Major equipment capital costs

Equipment Tag	Equipment Type	Bare Module Cost	Scaled Bare Module Cost
T-101	Absorber	$1,460,000	$1,460,000
T-102	Stripper	$332,000	$332,000
S-101 - S-120	Storage Tanks	$879,000	$17,580,000
S-121 - S-125	Storage Tanks	$430,000	$2,150,000
H-201	Fired Heater	$23,100,00	$35,905,158
M-201	In-Line Mixer	$685,000	$685,000
R-201	Autothermal Reformer	$299,000	$1,037,947
R-301	WGS Reactor	$545,000	$616,643
R-302	WGS Reactor	$545,000	$546,857
V-401	Flash Drum	$1,870,000	$1,870,000
V-402	Flash Drum	$2,130,000	$2,130,000
T-401	Absorber	$32,000,000	$27,783,731
T-402	Stripper	$42,400,000	$54,657,508
S-401 - S-410	Storage Tanks	$594,000	$5,940,000
S-501 - S-506	Holding Tanks	$415,000	$2,490,000
B-501A - B-504A	Packed Bed Towers	$30,514,525	$118,894,141
B-501B - B-504B	Packed Bed Towers	$30,514,525	$118,894,141
S-601 - S-620	Holding Tanks	$430,000	$8,600,000
		Total:	**$400,005,244**

Table 6.1-2 Heat exchanger capital costs

Equipment Tag	Equipment Type	Heat Transfer Area (m^2)	Bare Module Cost
E-101	Shell/Tube Heat Exchanger	173	$433,000
E-102	Condenser	47	$259,000
E-103	Kettle Reboiler	111	$1,352,065
E-201	Shell/Tube Heat Exchanger	278	$598,000
E-301	Shell/Tube Heat Exchanger	431	$838,000
E-401	Shell/Tube Heat Exchanger	2190	$3,201,080
E-402	Shell/Tube Heat Exchanger	2920	$3,823,189
E-403	Condenser	2150	$3,181,699
E-404	Kettle Reboiler	17600	$11,060,687
E-405	Shell/Tube Heat Exchanger	6770	$8,600,345
E-406	Shell/Tube Heat Exchanger	22900	$38,222,064
E-501	Condenser	200	$471,000
E-502	Shell/Tube Heat Exchanger	200	$473,000
E-601	Shell/Tube Heat Exchanger	528	$985,000
E-602	Shell/Tube Heat Exchanger	481	$917,000
E-603	Shell/Tube Heat Exchanger	566	$1,070,000
E-604	Shell/Tube Heat Exchanger	827	$1,560,000
		Total:	**$77,045,128**

Table 6.1-3 Pumps and compressors capital costs

Equipment Tag	Equipment Type	Power (MW)	Bare Module Cost
C-101	Centrifugal Compressor	8.91	$13,854,445
P-101	Centrifugal Pump	0.00139	$39,500
P-102	Centrifugal Pump	0.165	$254,000
C-201	Centrifugal Turbine	-1.61	$4,740,000
P-201	Centrifugal Pump	0.191	$284,000
C-401	Centrifugal Turbine	-23.9	$57,439,667
P-401	Centrifugal Pump	0.298	$302,000
C-501	Centrifugal Compressor	5.73	$10,630,539
C-601	Centrifugal Compressor	12.4	$50,680,020
		Total:	**$138,234,171**

Table 6.1-4 Summary of total capital costs

Item	Cost
Major Equipment	$400,005,244
Heat Exchangers	$77,045,128
Pumps and Compressors	$138,234,171
Total Equipment Cost	**$615,284,543**
Total Grassroots Module Cost	**$819,875,618**
Working Capital Cost	**$92,292,682**
Total Capital Investment	**$912,168,299**

6.2 Operating Costs

The operating costs for this plant consist of raw materials, utilities, and labor costs and are estimated to be about $327 million annually, summarized in Table 6.2-1. Raw materials make up the bulk of these operating costs, as this process requires large amounts of natural gas, one of

the most costly materials. Raw material costs were estimated using vendor data and current

natural gas prices in the U.S. averaged over the past year. Amine costs consist of the makeup

streams required according to losses calculated in Aspen, as well as one full year of fresh amines,

while natural gas and oxygen costs are the calculated feed costs necessary for our production

goals. These costs are given in Table 6.2-2.

Table 6.2-1 Summary of total operating costs

Item	Total Cost
Raw Materials	$422,656,788
Utilities	$89,935,499
Labor	$5,739,552
Total:	**$518,331,839**

Table 6.2-2 Summary of raw materials costs

Component	Amount Required	Unit	Cost per Unit	Total Cost
Natural Gas	1,154,828,160	kg	$0.28	$323,351,885
O_2	990,917,280	kg	$0.10	$99,091,728
MDEA	34,779	kg	$1.00	$34,779
MEA	119,729	kg	$1.49	$178,396
			Total:	**$422,656,788**

Utilities costs are the second most expensive because of the large amounts of cooling

water and electricity required. Prices per unit for each utility were based on those provided by

Turton et al. (2012) and are summarized in Table 6.2-3. The total utility costs for each unit

operation, broken down by utility type, are given in Table 6.2-4. Negative numbers indicate

utilities that are being produced and sold. Steam from both water-gas shift reactors at 75°C and

155°C is being sold to reduce utility costs, and electricity produced in the ATR and second amine scrubbing unit.

Table 6.2-3 Summary of utilities pricing

Utility	Price per Unit
Electricity	$0.045 / kWh
Cooling Water	$0.08 / tonne
Process Water	$0.53 / tonne
Steam	$4.40 / tonne
Wastewater Disposal	$0.53 / tonne
Hazardous Waste Disposal	$145 / tonne

Table 6.2-4 Summary of utilities costs

Block	Cost per Year						
	Electricity	Steam	Cooling Water	Process Water	Wastewater Disposal	Hazardous Waste Disposal	Total Cost
AS1	$3,380,593	$7,682,833	$403,243	$4,021	$0	$6,783,846	$18,254,536
ATR	-$502,637	$0	$66,240	$1,019,851	$0	$0	$583,454
WGS	$0	-$6,739,920	$122,544	$0	$0	$0	-$6,617,376
AS2	-8,354,400	$1,609,817	$75,546,903	$51,079	$494,630	$0	$69,348,029
PSA	$2,134,998	$0	$4.65	$0	$0	$0	$2,135,003
CO_2 Comp	$4,389,228	$0	$1,842,625	$0	$0	$0	$6,231,853
						Total:	$89,935,499

Labor costs were calculated by first estimating the number of operators required per shift according to Equation 6.2-1, provided by Turton et al. (2012). N_{np} is the number of

non-particulate solids process units and P is the number of particulate solid units, which was zero in all cases.

$$N_{OL} = (6.29 + 31.7P^2 + 0.23N_{np})^{0.5}$$
<div align="right">Eqn. 6.2-1</div>

18 workers per shift are needed for operation and assuming five full-time employees per operation, this gives a total of 90 operators required. An hourly wage of $36.40 was assumed based on the average wage for chemical processing facilities provided by Turton et al. (2012), adjusted for inflation. This plant operates 24 hours per day, 345 days out of the year, resulting in an annual labor cost of $5,739,552.

6.3 Projected Revenues

Given that blue hydrogen makes up only a small percentage of the hydrogen that is produced in the U.S. and globally, little data exists on the typical price for this product. We set our price based on estimates outlined by the U.S. Department of Energy, which listed $5 per kg as the typical cost of hydrogen produced from clean energy (U.S. Department of Energy, n.d.). By comparison, traditional gray hydrogen today costs around $1.50 - $2 per kg (Clifford, 2022). In line with clean energy estimates, $5 per kg was chosen as the sale price for our blue hydrogen. This plant produces 30,662 kg H_2 per hour, or almost 254 million kg per year, bringing in a total revenue of a little over $1.2 billion annually. CO_2 provides a second source of revenue, although it is much smaller in scale. CO_2 sold for enhanced oil recovery (EOR) typically sells for 40% of the per-barrel oil price, which is roughly $85 averaged over the past year in the U.S. (Edwards & Celia, 2018). At this rate, we plan to sell our CO_2 at $34 per tonne. This plant generates almost 2.5 billion kg of CO_2 annually, bringing in a revenue of $84.5 million. Together, our annual revenue is projected to be almost $1.4 billion. Table 6.3-1 summarizes these revenue sources.

Table 6.3-1 Summary of sources of revenue

Revenue Source	Amount Sold per Year (kg)	Unit Price	Annual Revenue
Hydrogen	253,881,360	$5 / kg	$1,269,400,000
Carbon Dioxide	2,485,275,120	$34 / tonne	$84,500,000
		Total:	**$1,353,906,800**

6.4 Taxes, Financing, and Assumptions

In order to fund the plant's estimated total capital investment (TCI) of almost $913 million, it will be fully financed with no down payment at an interest rate of 3%. A 10 year loan at this rate would accrue about $145 million in interest bringing the total loan amount to $1,056,955,803. The loan repayment schedule was calculated using an amortization schedule creating equal payments on the sum of the interest and principal payments each period. While this interest rate is lower than the current U.S. Federal Reserve rate of 4.83%, the plant would receive a favorable loan rate (The Federal Reserve, 2023). This is common for megaprojects, particularly those that will bring jobs and industry to an area. Additionally, incentives for hydrogen production and carbon capture could contribute to a favorable loan rate. These loans could be sourced from the state or national government as well as through private investment banks. Payments on the loan would not start until the conclusion of year two. Operations are not scheduled to begin full production until the end of year two so there would be a grace period until this begins. Construction is projected to take 18 months with the following 6 months to begin startup and establish procedures. All operating costs in the second half of year two are to be paid in full, while revenue for that period would be cut in half because of startup operations.

Based on the plant's location in Midland, Texas it is subject to a number of local and national taxes. After 18 months and completion of construction, the plant is subject to the local

property tax of about 1.207% (Midland Development Corporation, n.d.). Property tax is taken as a fraction of the initial book value of the plant which comes out to about $7.54 million per year. Despite a decrease in book value from depreciation, it is assumed that property tax will remain the same through the life of the plant. Even if the plant is not producing any revenue, property tax is still assessed as it pays for much of the local services including hospitals and schools. Once the plant generates any revenue, it is subject to a Texas corporate franchise tax of 1% on all revenue after property tax is deducted (Midland Development Corporation, n.d.). Annual franchise tax of a normal operating year is roughly $13.4 million. There is a sales and use tax in Texas, but manufacturing plants are exempt. Finally, once profits are generated, the firm will be subject to a federal corporate tax on profits. The current federal corporate tax rate is 21% applied to profits which is a historic low (Trading Economics, n.d.). Taxable income to this rate is calculated as profits (operating costs subtracted from revenue) with the aforementioned property and franchise taxes deducted. Additionally, in years 2-12 of the plant's life, depreciation and interest payments on the loan are included as tax write-offs decreasing the taxable income. Depreciation was calculated as a straight line depreciation over the course of 10 years which began after year two. Once the federal taxes are calculated, available tax credits may be applied. Because of the plant's reuse of carbon via carbon sequestration for EOR, it is eligible for tax credits as defined by the Inflation Reduction Act (Jones & Sherlock, 2021). After 2026, this comes out to $35 per tonne. At steady state rates, this comes out to about $87 million in tax credits per year.

6.5 Cash Flow Analysis

Table 6.5-1 Cash Flow Scenarios

Scenario	Simple Payback Period	IRR	Cumulative DCF
Default	3.5 years	18.6%	$4,795,878,564
2x Natural Gas Price	5 years	12.6%	$2,552,650,057
3x Natural Gas Price	16 years	3.9%	-$192,781,778
$3/kg Hydrogen Price	7 years	8.6%	$1,157,243,170
$10/kg Hydrogen Price	2.5 years	33.1%	$271,798,237,783
$3/kg Hydrogen Price 1.5x Natural Gas Price	16.5 years	3.6%	-$241,744,255

In Table 6.5-1, different cash flow scenarios are outlined with assumed profitability and different market operating conditions. The default scenario is outlined in this paper using the numbers from the sections capital costs, operating costs, projected revenues, and financing. The simple payback period is the number of years when the total cash flow is zero or the profits generated are equal to the total capital investment. A faster or lower payback period is favorable. Internal rate of return (IRR) is the discount rate required so that net present value (NPV) is equal to zero. NPV takes the yearly profit and adjusts it via the discount rate into present dollars given the number of periods that have passed. When NPV is zero, a firm has broken even on its initial investment as adjusted for present dollars. A higher IRR is deemed to be a greater return on initial investment. Discounted cash flow (DCF) is the value of each year's cash flow as adjusted via a discount rate for present value dollars. For example, after the plant reaches steady state where the loan is paid off and depreciation completes, the yearly profit will remain the same, while the discounted cash flow will decrease each year because of the discount rate. This

represents the declining present value of money year after year. Cumulative DCF is the sum of every year's DCF including the total capital investment. Working capital is added on at the end as it is assumed to be sold off at the end of the plant's life. A discount rate of 10% was chosen for all scenarios to calculate DCF. Higher Cumulative DCF is favorable because it represents how much cash flow the plant will generate.

The default scenario is considered highly profitable with a payback in 3.5 years and IRR of 18.6%. It is considered worthwhile for a large capital project, such as a plant, to be built if it can pay back within five years if the only target is to maximize profits. Targets other than profits could be job creation, technology investment, need for in-house production of feedstock and a host of other reasons where the profit of the project is not the primary concern and a longer payback period is acceptable. In the other scenarios, the two manipulated variables were the price of natural gas and the price of hydrogen. Natural gas makes up 76.5% of costs and is a notoriously volatile commodity with prices rapidly rising and falling being impacted by a range of factors from geopolitical instability to weather events. Hydrogen prices account for 93.76% of revenue so any price fluctuations would greatly impact the fate of the plant. A double natural gas price is considered the limit of a realistic conservative scenario as U.S. natural gas prices between 2001-2022 have at max been 80% greater than our base case scenario for a single year (*United States Natural Gas Industrial Price (Dollars per Thousand Cubic Feet)*, n.d.). In this year's range, prices have been about 2% greater than our estimate on average. No single month of the year has been three times our natural gas price. Even in that listed scenario, while difficult, the plant is still able to eventually generate profit. Another realistic conservative scenario is the combination of a 1.5x price hike in natural gas prices and a $3/kg hydrogen price of or 40% price drop from our $5/kg estimate. This scenario is even more detrimental than a 3x natural gas

price increase. While still generating profit, it would be hard to justify the plant as an investment if profits are the sole reasoning.

The default scenario was deemed the most realistic scenario based on current data from the U.S. Energy Information Agency. Aside from the $10/kg hydrogen price scenario, every other scenario is more conservative than the base case. While the base case is profitable, it is important to show that even under austere conditions, the plant could survive and remain profitable. It is important to note, however, that in the austere economic environment there would be several years of negative profits until the plant may break even. These scenarios would require further financing and investment to stay afloat.

6.6 Market Analysis and Future Profitability

In the cash flow analysis, it is highlighted that the two economic variables that impact the plant the most are the prices of natural gas and hydrogen. While natural gas prices are considerably volatile, there is at least a highly developed global market with ample domestic reserves and production. Hydrogen, on the other hand, does not have nearly as much of a developed global interconnectivity or market growth rate. The current main usage for hydrogen fuel is in ammonia production and hydrocarbon refining (*The Future of Hydrogen – Analysis*, n.d.). These industries are fairly mature and won't see a dramatic increase in production and associated demand in hydrogen production. New innovations such as hydrogen fuel cells and hydrogen storage may alter demand and rapidly increase prices and market growth. Additionally, China and the Middle East command more demand for hydrogen than the United States (Muritala et al., 2019). There is no developed international pipeline network for hydrogen or extensive liquid hydrogen exports. Development of this infrastructure could contribute to an increase of demand for a U.S. plant. With the Department of Energy citing the price of hydrogen

as $5 per kilogram, there is a concerted effort to bring this closer to $1/kg (*Hydrogen Shot*, n.d.). Government regulations and subsidies would have a substantial impact on the profitability of the plant. Future possible legislation such as a carbon tax, hydrogen subsidies, and tax credits could have profound impacts on the economics of the plant.

6.7 Conclusions

Based on the economic analysis, there are multiple scenarios that would yield very favorable profits if the plant was invested in, even if profits are the only concern. Even in the extremely conservative scenarios, the plant is able to generate profits and break even on the initial investment. However, the market analysis shows there are a host of different variables, including government regulation and market changes, that could affect the future of such an investment. Some of these variables are nearly impossible to model or predict. There is considerable uncertainty and risk in having unknown variables that severely affect the plants profitability.

7. Safety, Environmental, and Societal Considerations

7.1 Safety Considerations

This process has many safety hazards and issues associated with it that stem from the hazardous nature of chemicals used and the extreme operating conditions of equipment. Several chemicals in the process are hazardous to human health, including carbon monoxide (CO), hydrogen sulfide (H_2S) and monoethanolamine (MEA), and several pose severe flammability and explosion hazards, including hydrogen (H_2), methane (CH_4), heavier hydrocarbons, and CO.

Chemical Hazards and Compatibility

CO is an intermediate formed in this process that is toxic if inhaled, can cause organ damage through prolonged, repeated exposure and is highly flammable (Sigma-Aldrich, 2023). The TLV-TWA, or the level at which workers may be repeatedly exposed without adverse effects, is 25 ppm. CO_2, while not as toxic or flammable as CO, also poses a threat as a simple asphyxiant because it can displace oxygen and cause suffocation and has a TLV-TWA of 5000 ppm (Sigma-Aldrich, 2021). Preventing the build-up and leakage of CO and CO_2, especially in areas of potentially high concentration, such as the CO_2 removal and compression units, is very important. H_2S is an extremely toxic and flammable gas that is fatal if inhaled, with a very low TLV-TWA of 1 ppm (Sigma-Aldrich, 2021). Although this process produces only small amounts of H_2S each day, the utmost care must be taken to prevent operator exposure. Both MEA and MDEA, the solvents used in both amine scrubbing units, pose health hazards as well. MEA can cause severe skin burns and eye damage, is harmful if inhaled, may cause respiratory irritation and is also a flammable and combustible liquid, while MDEA may cause serious eye irritation (ThermoFisher Scientific, 2021).

To mitigate hazards from all of these chemicals, proper PPE will be worn at all times by employees, including flame retardant clothing, gloves, safety glasses, hard hats, and respirators where necessary. Eye wash stations and emergency showers will be placed around the facility as well in case of exposure. To minimize risk of exposure, gas detection systems, proper ventilation, emergency shut-offs and interlocks, and alarm systems will be used extensively throughout the plant and regular maintenance and inspection will be conducted to detect corrosion and leaks before they lead to loss of primary containment.

In addition to hazards posed by single components, several chemicals are incompatible with each other and should be kept separate at all times. Figure 7.1-1 provides a table compiled from CAMEO Chemicals listing the compatibilities between chemicals used throughout this process. H_2S has several incompatibilities, including with water in which it will react to form sulfuric acid, a toxic and corrosive liquid that is dangerous to humans and equipment. This reaction is also highly exothermic, leading to a dangerous release of heat if uncontained. H_2S has similarly dangerous reactions with CO_2, O_2, MEA, and MDEA in which potentially flammable gas is generated in exothermic reactions. H_2S is removed at the beginning of the process to avoid any risk of mixing between these components, although it will still need to be carefully isolated and disposed of after it has been removed to prevent accidental contamination. Oxygen is largely incompatible with almost every compound in this process as the hydrocarbons and most gasses are combustible. Oxygen acts as an oxidizer, fueling fires and explosions. Combustion of chemicals is desired in the controlled environment of the ATR, but could have devastating consequences if it occurs during a loss of primary containment. To prevent incompatible mixing, emergency interlocks, remote shut-off systems, and proper labeling of piping and vessels will be used throughout the facility.

Figure 7.1-1 CAMEO Chemicals compatibility chart for all compounds in the process

Equipment and Process Hazards

In addition to chemical hazards, this process poses many equipment hazards as well. Although none of the chemicals used are extremely corrosive by nature, corrosion may still occur as the facility ages or due to unexpected mixing of chemicals. Additionally, hydrogen embrittlement is a corrosive hazard to piping, as hydrogen is small enough to diffuse into metals like steel. Corrosion-resistant materials, such as type 316 stainless steel, were chosen for much of the equipment in this operation to prevent leaks and cracks, but regular thorough inspection is still required. Inspection will be needed to check for fouling in pipes and heat exchangers as well.

Leak formation in any part of the process is especially dangerous given that much of the process stream is highly flammable. H_2, CH_4, ethane, propane, and butane are all extremely flammable compounds that pose fire and explosion risks. If a loss of containment occurs, vapor clouds may form that could easily find an ignition source leading to a fire or deflagration with the potential to damage not only the facility but also the surrounding community. Deluge and emergency water systems will be in place that can be activated in the event of a vapor cloud release and remote shut-off systems will be used to prevent further leakage once it is detected. Interlocks, relief valves with containment systems, and flares are additional mitigative safety measures that could be used to prevent catastrophic failure.

Runaway reactions are another large threat to this process, given that both the combustion reactions in the ATR and the water-gas shift reactions are exothermic. Emergency relief systems and several back-up cooling systems will be in place to prevent runaway reactions and the failure of a reactor. Overpressure in reactors, holding tanks, and other equipment is a safety concern that can be prevented with pressure monitoring systems and alarms, as well as relief valves.

Additional equipment failures, such as valve and seal leaks in pumps and compressors, will be prevented through regular inspection and maintenance and mitigated through relief valves and containment systems. As mentioned above, rigorous gas detection systems will be used not only for toxic compounds but also for highly flammable gasses like H_2 and CH_4.

A high risk regular step is the loading, storage, and formation of the liquid CO_2 product. In the storage and internal transportation through the plant, any undetected leak can be extremely dangerous. Gaseous CO_2 poses a unique risk because of its ability to displace oxygen at ground level because it is heavier than air. An undetected leak in an enclosed space can be an extreme hazard to operators as they can suffocate from lack of oxygen resulting in headaches, dizziness, and possibly even death. This risk can be mitigated by regular air testing of air composition, steady flow rates, regular maintenance of piping, and portable air alarms for operators. While the hydrogen production is pipelined out of the site, product CO_2 used for EOR will have a variety of destinations for EOR so it will have to be transported via truck out of the plant. Transporting CO_2 products via truck also presents its own unique challenges.

In order to prevent serious process safety incidents from occurring, a strong safety culture will need to be established in the facility. Appropriate PPE, including flame retardant clothing, is crucial for every operator to wear. Emergency and evacuation plans will be established and practiced in preparation for a serious incident. Near miss reporting is an important practice so that even minor incidents can be investigated and resolved. Sufficient training, open communication, and enforcement of protocols are crucial to creating a safe work environment and attention to safety is a responsibility shared by all levels of employees and management at the facility.

7.2 Environmental Considerations

Greenhouse Gas Emissions and Fossil Fuels

Although blue hydrogen is seen as a more environmentally-conscious means of hydrogen production than traditional gray hydrogen, there are still many climate and environmental concerns throughout the process. First of all, this process does not lessen society's dependence on fossil fuels, instead relying on natural gas extracted from the ground as its feedstock. Fossil fuels are nonrenewable resources that release greenhouse gasses when burned, contributing to global warming and as such, are undesirable and unsustainable as energy sources in the future. This process relies on and supports the continued extraction of natural gas, and other fossil fuels through enhanced oil recovery, lending itself a very large carbon footprint.

CO_2 is the most ubiquitous greenhouse gas emitted today, trapping heat in the atmosphere that has contributed significantly to the 1.1°C of global warming that has already occurred (Lindsey & Dahlman 2022). While our process captures the CO_2 produced instead of releasing it into the atmosphere, there is still the potential for leaks in the process and the release of CO_2 during the burning of waste streams. Amine scrubbing captures 96.2% of the CO_2 produced throughout our process, but the remaining 7,514 kg/hr is left in the waste stream at the end of the process to be burned, which means this facility still emits about 180 metric tonnes of CO_2 per day or almost 62,300 metric tonnes per year, leaving much room for improvement.

Methane is another greenhouse gas central to this process. Methane is more than 25 times more potent than CO_2 in its warming potential, although its atmospheric lifetime is shorter, on the scale of decades compared to centuries for CO_2 (U.S. Environmental Protection Agency, 2022). Although it's outside the scope of this project, the extraction of methane poses many environmental problems, as a sizable portion of the methane that's produced in the U.S. is leaked

into the atmosphere either during extraction, transportation, or storage. Additionally, a sizable portion of the methane used in this process remains unreacted (roughly 12,000 kg/hr) and is also sent through the waste stream to be burned. Burning this methane produces additional CO_2 that will not be captured, reducing the "blueness" of this process and increasing the plant's carbon footprint.

Other Pollutants

Besides greenhouse gasses, other air pollutants exist in this process. H_2S is toxic to humans by itself but it also mixes with water to form sulfuric acid, another toxic and corrosive compound. If mixed with water vapor in the air, H_2S can contribute to the formation of acid rain, damaging plants, ecosystems, and human infrastructure . Additionally, formation or release of sulfuric acid at the ground level can damage aquatic ecosystems and acidify fresh groundwater sources, impacting both plants and animals (California Air Resources Board, n.d.). Although this process produces very small amounts of H_2S, it is still important to handle it correctly to reduce negative environmental impacts. CO is another compound toxic to humans but it also contributes to air pollution, as CO takes part in chemical reactions that form ground-level ozone (NASA, n.d.). Again, only a small percentage of CO is left in the tail gas at the end of our process, but given the large quantities of gas processed each day, it is an important consideration.

Additional environmental concerns include the air quality surrounding the plant, not only from CO and H_2S, but also from the burning of hydrocarbons and other gasses in general. Unexpected uses of flares and relief valves may also contribute to the release of greenhouse gasses and air pollutants. Heat pollution may be a concern as much of this process is exothermic and a lot of heat will be removed in the form of steam which will need to be disposed of. Excess

heat pollution may detrimentally affect surrounding ecosystems, although this facility is located in Texas which is likely already adapted to warmer temperatures.

7.3 Societal Considerations

The goal of the "blue" hydrogen process is to act as a stepping stone towards cleaner hydrogen production while green, completely renewable means of hydrogen production are still being developed. Hydrogen has many uses today in the chemical industry for products such as ammonia, but it may also see growing demand in the near future for electricity applications as fuel cells become increasingly commercially viable. With the advent of a proposed "hydrogen economy," in which hydrogen could become the basis of our nation's energy supply instead of fossil fuels, the search for less carbon intensive means of hydrogen production has intensified. Although blue hydrogen is not the most environmentally-conscious form of production it is an important short-term solution while green hydrogen production is scaled-up for industrial use.

Community Impacts

In terms of the local community surrounding this facility, concerns may include pollution and emergency situations. Air pollution may be a concern as discussed above, as well as heat pollution and even noise pollution from heavy machinery running throughout the day. Included in air pollution may be foul odors from H_2S and CH_4 which usually have unpleasant, but harmless odors associated with them. This facility will require significant land area to accommodate very large unit operations and to provide enough space between equipment to reduce potential safety hazards. The facility will ideally be cited in an industrial area, far away from neighborhoods, to avoid excess disruption to the community. In the event of explosions, fires, or evacuations, the surrounding community and businesses may be damaged and negatively impacted.

8. Conclusions and Recommendations

Conclusions

Though the concept of blue hydrogen production via ATR has existed for some time now, this industry-scale design attempts to further prove the profitability of blue hydrogen production through thorough economic analysis. Our design also provides an extremely high hydrogen to CO_2 output ratio, even for blue hydrogen production facilities, which typically output around four kg CO_2 per kg H_2 while our design releases around 1.5 kg CO_2 per kg H_2 (Moberg, 2022). This plan allows for the production of over 250 million kg of hydrogen per year with an estimated revenue greater than $1.3 billion.

While this process does draw a huge revenue stream, it is a massive project that requires many units and materials to run smoothly. The plant requires natural gas, amines, such as MEA and MDEA, pure oxygen, and massive amounts of process and cooling water; and each of these materials must be stored and input at proper pressures, temperatures, and placement within the final process. Amines are used in two separate steps to clean H_2S from the natural gas stream and then CO_2 from the gasses output by the ATR and WGS reactors. Water, which is reacted with methane and CO to form hydrogen, is mixed into the natural gas stream prior to the reactors. Finally, oxygen is required to combust methane and raise the heat duty of the ATR to 0 MW. Produced hydrogen is meant to be sold directly, by pipeline, to a nearby ammonia facility where it will be reacted with nitrogen to produce ammonia. The captured carbon dioxide will also be liquified and sold to oil fields for use in EOR where it can be pumped underground to optimize oilfield oil recovery.

The environmental and social impacts of this design and the plant are mainly positive, though the plant itself, barring its relationship with other hydrogen production methods, does

have some negatives. First, this plant draws a massive amount of both process water and cooling water. This water must be fresh, thus further contributing to the worldwide issue of freshwater access. Furthermore, though this plant does capture almost all of the CO_2 that it produces, electricity used within the plant, and energy and materials used to build this plant are likely associated with massive CO_2 emissions. However, with this plant design in place, more hydrogen can be produced cleanly, pulling the market away from hydrogen production techniques that are far less environmentally friendly. The provided economic analysis also shows that this type of hydrogen production facility could be highly propitious, which should lead to a large market development around blue hydrogen. While our analysis and design of this plant shows favorable results, the limited time and resources that we have available to our team introduced some limitations to our study. Thus, the following section outlines these limitations so that future teams can further analyze and refine our design.

Recommendations

In the first amine scrubber to remove hydrogen sulfide, our Aspen model could be improved to further increase our design accuracy. Getting a functional cross heat exchanger into our Aspen model would allow for improved testing and simulation in the real plant, and would decrease heating costs of the unit. The Aspen model also currently does not have a functional recycle stream, and calculations had to be done by hand. Repairing this problem would allow for easy simulation of the unit and save time in testing for the real plant. The overall unit could also be improved with more optimization of tray sizing, operating temperatures and pressures, reboiler rates, and reflux ratios.

Our second amine scrubber also has some deficiencies that need to be addressed. The current process requires $69 million each year in utility costs alone, due to the process generating

excessive amounts of heat. This decreases the efficacy of the heat exchangers within the unit, which already contribute significantly to the overall capital costs of the plant. The stripper reboiler duty is also extremely high at over 1000 MW. This could be an unavoidable consequence of the sheer size of the unit, but could possibly be optimized to decrease its size. An alternative to this is reducing the CO_2 capture rate, but this must be done with blue hydrogen regulations in mind. Future work could consider using multiple amine scrubber units for CO_2 capture to distribute the heat duties required and decrease size, but this would make the process much more complex while greatly increasing capital costs.

There are some improvements that could be made to the ATR unit that potentially improve conversion and decrease capital costs. Our Aspen model of the ATR currently treats each reaction within the unit as occurring in series, but in a real ATR unit these reactions would all be occurring in parallel. Combining these reactions into a model would improve realism and potentially change design parameters such as the sizing of the unit. Due to these reactions taking place in series within the model, the size we have designed for may actually be larger than an ATR in the actual plant. This would decrease capital costs for the unit and catalyst within. Additionally, future work should test different catalysts for use in the ATR, as our catalyst was chosen to match rate equations provided by Xu & Froment (1989). Another catalyst could potentially be more optimized for use in this specific unit and increase the efficiency of the overall plant. Smaller improvements and fine tuning of feed inputs can also be performed to ensure that this critical unit of our plant is operating at maximum efficiency.

One of the major problems with the current PSA unit is the lost product through the tail gas stream. The tail gas is around 68 mol% H_2, resulting in 166 tons of H_2 not being sold as product each operating day. This translates into about $830,000 lost revenue per operating day, or

$286 million per year (if H_2 is priced at $5/kg). This is mainly due to the PSA's roughly 82% recovery of hydrogen, and our feed being 92 mol% H_2 to begin with. To rectify this, future work could simply include more PSA beds that recover additional hydrogen from the tail gas stream. This would significantly increase capital costs, but the future revenue from this improvement could justify the investment. Including additional PSA beds would decrease the amount of tail gas available to burn, so energy requirements should be taken into account across the plant when implementing this solution.

The water gas shift unit could potentially make up for this loss in heat energy, as the heat removed from the process is not fully integrated to provide the plant with additional energy. The unit currently produces 85,000 kg/hr of steam, which is then sold to produce $6.7 million in additional revenue. However, both amine scrubbers require a total of $9.9 million per year to buy steam from an outside source. Utilizing the steam produced from within the plant could significantly decrease utility costs and allow for more energy flexibility as the plant decreases its reliance on outside energy. Additionally, the high temperature reactor currently produces very low temperature steam that is difficult to use. Future work could attempt to design this reactor to produce more useful, higher temperature steam.

Our CO_2 compression unit is fairly simple, but could be further optimized by increasing the number of stages. However, this could encounter a diminishing returns effect where power requirements are too great at a certain number of stages. Future work could consider adding stages, but this would all depend on who the CO_2 is being sold to. Depending on the buyer, it may be beneficial to add stages to increase differential pressure, or it could be more beneficial to decrease the temperature of the product instead.

9. Acknowledgements

We would like to thank our advisor, Professor Eric Anderson of the Chemical Engineering department, for his continued support and guidance throughout this design project. We would also like to thank Professor Ron Unnerstall of the Chemical Engineering department for his contributions and advice stemming from his extensive experience in the oil and gas industry as well as his knowledge of process safety.

10. References

Adams II, T. A. and Barton, P. I. (2009). A dynamic two-dimensional heterogeneous model for water gas shift reactors. *International Journal of Hydrogen Energy, 34*, 8877–8891. doi:10.1016/j.ijhydene.2009.08.045

Afkhamipour, M., & Mofarahi, M. (2017). Review on the mass transfer performance of CO_2 absorption by amine-based solvents in low- and high-pressure absorption packed columns. *RSC Adv.*, *7*(29), 17857–17872. https://doi.org/10.1039/C7RA01352C

Amine Scrubbing System Overview—How Amine Treating Works. (n.d.). Retrieved March 14, 2023, from https://www.carverpump.com/amine-scrubbing-system-overview/

Ayastuy, J. L., Gutiérrez-Ortiz, M. A., González-Marcos, J. A., Aranzabal, A., & González-Velasco, J. R. (2004). Kinetics of the low-temperature WGS reaction over a $CuO/ZnO/Al_2O_3$ Catalyst. *Industrial & Engineering Chemistry Research*, *44*(1), 41–50. https://doi.org/10.1021/ie049886w

Baksch, M., & Ackley, M. (2002). *Pressure Swing Adsorption Process for the Production of Hydrogen* (Patent No. US 6,340,382).

Benyahia, F., & O'Neill, K. E. (2005). Enhanced voidage correlations for packed beds of various particle shapes and sizes. *Particulate Science and Technology*, *23*(2), 169–177. https://doi.org/10.1080/02726350590922242

California Air Resources Board. (n.d.). *Hydrogen Sulfide & Health*. California Air Resources Board. Retrieved March 16, 2023, from

https://ww2.arb.ca.gov/resources/hydrogen-sulfide-and-health

Capello, C., Fischer, U., & Hungerbühler, K. (2007). What is a green solvent? A comprehensive

framework for the environmental assessment of solvents. *Green Chemistry*, *9*(9),

927–934. https://doi.org/10.1039/b617536h

Chai, S. Y. W., Ngu, L. H., & How, B. S. (2022). Review of carbon capture absorbents for CO_2

utilization. *Greenhouse Gases-Science and Technology*, *12*(3), 394–427.

https://doi.org/10.1002/ghg.2151

Chen, W.-H., & Chen, C.-Y. (2020). Water gas shift reaction for hydrogen production and carbon

dioxide capture: A review. *Applied Energy*, *258*, 114078.

https://doi.org/10.1016/j.apenergy.2019.114078

Clifford, C. (2022, January 6). *Hydrogen power is gaining momentum, but critics say it's neither*

efficient nor green enough. CNBC.

https://www.cnbc.com/2022/01/06/what-is-green-hydrogen-vs-blue-hydrogen-and-why-it

-matters.html

Duplex stainless steel reactors. TITAN Metal Fabricators. (2021, December 20). Retrieved

February 13, 2023, from

https://www.titanmf.com/products/reactors/duplex-stainless-steel-reactors/

Economic Indicators. (2022). *Chemical Engineering, 129*(9), 52.

https://proxy1.library.virginia.edu/login?qurl=https%3A%2F%2Fwww.proquest.com%2F

trade-journals%2Feconomic-indicators%2Fdocview%2F2712894254%2Fse-2%3Faccou

ntid%3D14678

Edwards, R. W., & Celia, M. A. (2018). Infrastructure to enable deployment of carbon capture, utilization, and storage in the United States. *Proceedings of the National Academy of Sciences*, *115*(38), E8815–E8824. https://doi.org/10.1073/pnas.1806504115

Eide-Haugmo, I., Lepaumier, H., Einbu, A., Vernstad, K., Silva, E., & Svendsen, H. (2011). Chemical stability and biodegradability of new solvents for CO_2 capture. *Energy Procedia, 4*, 1631-1636. 10.1016/j.egypro.2011.02.034.

Garcia, M., Knuutila, H. K., Gu, S. (2017). Aspen Plus simulation model for CO_2 removal with MEA: Validation of desorption model with experimental data. *Journal of Environmental Chemical Engineering*, *5*(5), 4693-4701. https://doi.org/10.1016/j.jece.2017.08.024.

Hikita, H., Asai, S., Ishikawa, H., & Honda, M. (1997) The kinetics of reactions of carbon dioxide with monoethanolamine, diethanolamine, and triethanolamine by a rapid mixing method. In Pinset, B.R., Pearson, L., and Rouchton, F.J.W. (Eds.), *Chem Eng. J.*, *13*, (pp. 7-12). Elsevier.

Hla, S. S., Park, D., Duffy, G. J., Edwards, J. H., Roberts, D. G., Ilyushechkin, A., Morpeth, L. D., & Nguyen, T. (2009). Kinetics of high-temperature water-gas shift reaction over two iron-based commercial catalysts using simulated coal-derived syngases. *Chemical Engineering Journal*, *146*(1), 148–154. https://doi.org/10.1016/j.cej.2008.09.023

Hoang, D., & Chan, S. (2004). Modeling of a catalytic autothermal methane reformer for fuel cell applications. *Applied Catalysis A: General*, *268*(1-2), 207–216. https://doi.org/10.1016/j.apcata.2004.03.056

Jassim, M. S. (2016). Sensitivity analyses and optimization of a gas sweetening plant for

hydrogen sulfide and carbon dioxide capture using methyldiethanolamine solutions. *Journal of Natural Gas Science and Engineering*, *36*, 175–183. https://doi.org/10.1016/j.jngse.2016.10.012

Jones, A., & Sherlock, M. (2021, June 8). The Tax Credit for Carbon Sequestration (Section 45Q). Congressional Research Service. (CRS Report No. IF11455) https://sgp.fas.org/crs/misc/IF11455.pdf

Lange, C., Berry, R., Magner, A., & Teevan-Kamhawi, F. (2020). *Carbon Capture, Utilization, and Storage from Power Plant Emissions* [Undergraduate Thesis]. University of Virginia.

Li, W., Chuah, C. Y., Kwon, S., Goh, K., Wang, R., Na, K., & Bae, T.-H. (2020). Nanosizing zeolite 5A fillers in mixed-matrix carbon molecular sieve membranes to improve gas separation performance. *Chemical Engineering Journal Advances*, *2*, 100016. https://doi.org/10.1016/j.ceja.2020.100016

Lindsey, R. & Dahlman, L. (2022). *Climate Change: Global Temperature*. National Oceanic and Atmospheric Administration. https://tinyurl.com/hnk7e2dn

Luneau, M., Gianotti, E., Guilhaume, N., Landrivon, E., Meunier, F. C., Mirodatos, C., & Schuurman, Y. (2017). Experiments and modeling of methane autothermal reforming over structured Ni–Rh-based si-sic foam catalysts. *Industrial & Engineering Chemistry Research*, *56*(45), 13165–13174. https://doi.org/10.1021/acs.iecr.7b01559

Mendes, D., Mendes, A., Madeira, L. M., Iulianelli, A., Sousa, J. M., & Basile, A. (2009). The water-gas shift reaction: From conventional catalytic systems to PD-based membrane

reactors-A Review. *Asia-Pacific Journal of Chemical Engineering*, 5(1), 111–137.

https://doi.org/10.1002/apj.364

Midland Development Corporation, -Golden Shovel Agency. (n.d.). *Local Tax Rates in Midland*.

Retrieved April 7, 2023, from

https://www.midlandtxedc.com/business-and-economy/local-tax-rates/

Moberg, J. (2022, January 28). *The Mirage of blue hydrogen is fading*. Green Hydrogen

Organisation. Retrieved April 6, 2023, from

https://gh2.org/blog/mirage-blue-hydrogen-fading

NASA. (n.d.). *Carbon monoxide, fires, and air pollution*. Earth Observatory. Retrieved March

16, 2023, from

https://earthobservatory.nasa.gov/images/7033/carbon-monoxide-fires-and-air-pollution#:

~:text=Like%20the%20burning%20of%20gasoline,that%20create%20ground%2Dlevel

%20ozone.

Oni, A. O., Anaya, K., Giwa, T., Di Lullo, G., & Kumar, A. (2022). Comparative assessment of

blue hydrogen from steam methane reforming, autothermal reforming, and natural gas

decomposition technologies for natural gas-producing regions. *Energy Conversion and

Management*, *254*, 115245. https://doi.org/10.1016/j.enconman.2022.115245

Peters, M. S., Timmerhaus, K. D., & West, R. E. (2003). *Plant Design and Economics for

Chemical Engineers*. 5th ed. New York: McGraw-Hill.

Pinsent, B.R.W., Pearson, L., & Roughton, F.J.W. (1956) The kinetics of combination of carbon

dioxide with hydroxide ions. Trans. Faraday Soc. 52, 1512-1520.

Price, S. (2022, March 19). *Fundamentals of gas-liquid absorption columns*. GlobalSpec.

   Retrieved March 14, 2023, from

   https://insights.globalspec.com/article/18294/fundamentals-of-gas-liquid-absorption-colu

   mns

Rochelle, G.T. (2009) Amine scrubbing for CO_2 capture. US National Library of Medicine

   National Institutes of Health. 325(5948):1652-4. doi: 10.1126/science.1176731.

San Marchi, C. (2005, March 17). *Technical reference on hydrogen compatibility of materials*.

   Sandia National Laboratories.

   https://h2tools.org/sites/default/files/2103TechRef_316SS.pdf

Sigma-Aldrich. (2021). *Carbon dioxide* [Safety data sheet].

   https://www.sigmaaldrich.com/US/en/sds/aldrich/295108

Sigma-Aldrich. (2023). *Carbon monoxide* [Safety data sheet].

   https://www.sigmaaldrich.com/US/en/sds/aldrich/295116

Sigma-Aldrich. (2021). *Hydrogen sulfide* [Safety data sheet].

   https://www.sigmaaldrich.com/US/en/sds/aldrich/295442

Sour Gas Handling Compliance. (n.d.). Texas Commission on Environmental Quality. Retrieved

   March 15, 2022, from

   https://www.tceq.texas.gov/assistance/industry/oil-and-gas/sour-gas-handling-compliance

The Federal Reserve. (2023, April 5). *Selected Interest Rates (Daily) - H.15*. Board of Governors

   of the Federal Reserve System. Retrieved April 6, 2023, from

   https://www.federalreserve.gov/releases/h15/

ThermoFisher Scientific. (2021). *Ethanolamine* [Safety Data Sheet].

https://www.fishersci.com/store/msds?partNumber=M2511&productDescription=ETHA

NOLAMINE+PURIFIED+1L&vendorId=VN00033897&countryCode=US&language=e

n

ThermoFisher Scientific. (2021). *N-Methyldiethanolamine* [Safety Data Sheet].

https://www.fishersci.com/store/msds?partNumber=AC126720010&productDescription=

N-METHYLDIETHANOLAMINE%2C+1KG&vendorId=VN00032119&countryCode=

US&language=en

Trading Economics. (n.d.). *United States Federal Corporate Tax Rate—2022 Data—2023*

Forecast. Trading Economics. Retrieved April 7, 2023, from

https://tradingeconomics.com/united-states/corporate-tax-rate

Turton, R., Bailie, R. C., Whiting, W. B., Shaeiwitz, J. A., & Bhattacharyya, D. (2012). Chapter

7. Estimation of Capital Costs. In *Analysis, synthesis, and design of Chemical Processes*

(4th ed.). Pearson Education.

U.S. Department of Energy. (n.d.). *Hydrogen Shot*. Office of Energy Efficiency and Renewable

Energy. Retrieved April 5, 2023, from

https://www.energy.gov/eere/fuelcells/hydrogen-shot

U.S. Environmental Protection Agency. (2022, June 9). *Importance of Methane*. EPA. Retrieved

March 16, 2023, from https://www.epa.gov/gmi/importance-methane

What is Alumina ? (n.d.). *Dynamic Adsorbents*. Retrieved February 27, 2023, from

https://www.dynamicadsorbents.com/alumina/what-is-alumina/

Xu, J., & Froment, G. F. (1989). Methane steam reforming, methanation and water-gas shift: I. Intrinsic Kinetics. *AIChE Journal*, *35*(1), 88–96. https://doi.org/10.1002/aic.690350109

Yavary, M., Ale Ebrahim, H., & Falamaki, C. (2016). Competitive adsorption equilibrium isotherms of CO, CO_2 , CH_4 , and H_2 on activated carbon and zeolite 5A for hydrogen purification. *Journal of Chemical & Engineering Data*, *61*(10), 3420–3427. https://doi.org/10.1021/acs.jced.6b00312

Yu, M.; Wang, K.; & Vredenburg, H. (2021). Insights into low-carbon hydrogen production methods: Green, blue and aqua hydrogen. *International Journal of Hydrogen Energy*, *46*(41), 21261–21273. 10.1016/j.ijhydene.2021.04.016.

Zhang, Y., Chen, C.C. (2013). Modeling CO_2 absorption and desorption by aqueous monoethanolamine solution with Aspen rate-based model. *Energy Procedia*, *37*, 1584-1596. https://doi.org/10.1016/j.egypro.2013.06.034.

11. Appendix

Sample Calculation 1 - Water Gas Shift Calculations

Water Shell Temperature and Flow Rate

$Q = AU_0\Delta T_{lm}$

$\Delta T_{lm} = Q/(AU_0) = (13{,}809{,}000 \text{ W})/[(353.4 \text{ m}^2)(300 \text{ W/m}^2\text{K})] = 130.2 \text{ K}$

  where A was calculated as the total surface area of the reactor, Q was determined by

  Aspen, and U_0 was assumed

$\Delta T_{lm} = 130.2 \text{ K} = \dfrac{T_1 - T_2}{ln(\frac{T_1 - T_b}{T_2 - T_b})} = \dfrac{400 - 400.1}{ln(\frac{400 - T_b}{400.1 - T_b})} \rightarrow T_b = 155°C$

$Q = m_c\Delta H_v$

$m_c = \dfrac{Q}{\Delta H} = \dfrac{13{,}809{,}000 \ W}{2{,}098{,}000 \ J/kg} = 6.58 \text{ kg/s} = 23{,}695 \text{ kg/hr} \rightarrow \sim 25{,}000 \text{ kg/hr}$

Sample Calculation 2 - PSA Bed Sizing

$V = \dfrac{SF}{n\rho\varepsilon}$

V- volume of bed (m^3)

S- size factor (kg packing/TPD H_2)

F- H_2 production capacity (TPD)

n- number of beds

ρ- average packing density (kg/m^3)

ε- average packing porosity

For our PSA system:

S = 3385.8 kg packing/TPD H_2

F = 750 TPD H_2

n = 8 beds

ρ = 1610.7 kg/m^3

ε = 0.386

$V = \dfrac{SF}{n\rho\varepsilon} \rightarrow V = \dfrac{3385.8 * 750}{8 * 1610.7 * 0.4} = 510.5 \text{ m}^3$

Sample Calculation 3 - Heat Exchanger Sizing

$Q = AU_0\Delta T_{lm}$

where Q and T were determined by Aspen and U_0 was assumed

$\Delta T_{lm} = \dfrac{(T_{H1} - T_{C1}) - (T_{H2} - T_{C2})}{ln(\frac{T_{H1} - T_{C1}}{T_{H2} - T_{C2}})} = \dfrac{(400 - 15) - (660 - 307.8)}{ln(\frac{400 - 15}{660 - 307.8})} = 368.36$ K

$A = Q/(U_0\Delta T_{lm})$

$A = (86.9MW) / [(850\ W/m^2K)(368.4K)] = 277.5\ m^2$

Sample Calculation 4 - Economics

$NPV = \dfrac{cash\ flow}{(1 + r)^t}$

$\dfrac{\$321,193,498}{(1+0.10)^{5\ years}} = \$501,487,876$

$Straight\ Line\ Depreciation = \dfrac{Purchase\ Cost - Salvage\ Value}{Useful\ Life}$

$\dfrac{\$615,284,543 - \$0}{10\ years} = \$61,528,454$ / year depreciation

Total Capital Investment = Grassroots Equipment Cost + Working Capital

$819,875,618 + \$92,292,681 = \$912,168,299

Taxes Paid = Tax Rate * (Revenue - Tax Deductions)

0.21 * ($814,721,094/yr - ($62,439,464/yr + $25,684,108/yr)) = $726,597,522